NAVAL POSTGRADUATE SCHOOL

MONTEREY, CALIFORNIA

THESIS

FREQUENCY AND POLARIZATION DIVERSITY JAMMING OF COMMUNICATIONS IN URBAN ENVIRONMENTS

by

Tuncay Ulama

September 2005

Thesis Advisor:	David C. Jenn
Second Reader:	Daniel C. Schleher

Approved for public release, distribution is unlimited

THIS PAGE INTENTIONALLY LEFT BLANK

REPORT DOCUMENTATION PAGE			Form Approved OMB No. 0704-0188
Public reporting burden for this collection of information is estimated to average 1 hour per response, including the time for reviewing instruction, searching existing data sources, gathering and maintaining the data needed, and completing and reviewing the collection of information. Send comments regarding this burden estimate or any other aspect of this collection of information, including suggestions for reducing this burden, to Washington headquarters Services, Directorate for Information Operations and Reports, 1215 Jefferson Davis Highway, Suite 1204, Arlington, VA 22202-4302, and to the Office of Management and Budget, Paperwork Reduction Project (0704-0188) Washington DC 20503.			
1. AGENCY USE ONLY *(Leave blank)*	**2. REPORT DATE** September 2005	**3. REPORT TYPE AND DATES COVERED** Master's Thesis	
4. TITLE AND SUBTITLE: Frequency and polarization diversity jamming of communications in urban environments			**5. FUNDING NUMBERS**
6. AUTHOR (S) Tuncay Ulama			
7. PERFORMING ORGANIZATION NAME (S) AND ADDRESS (ES) Naval Postgraduate School Monterey, CA 93943-5000			**8. PERFORMING ORGANIZATION REPORT NUMBER**
9. SPONSORING /MONITORING AGENCY NAME (S) AND ADDRESS (ES) N/A			**10. SPONSORING/MONITORING AGENCY REPORT NUMBER**
11. SUPPLEMENTARY NOTES The views expressed in this thesis are those of the author and do not reflect the official policy or position of the Department of Defense or the U.S. Government.			
12a. DISTRIBUTION / AVAILABILITY STATEMENT Distribution Statement (mix case letters)			**12b. DISTRIBUTION CODE**
13. ABSTRACT (maximum 200 words) The purpose of this research is to investigate how to exploit frequency and polarization techniques in reducing the effects of jamming against UAV relay communication links in an urban warfare environment. There have been early studies investigating the diversity techniques against multipath and fading problems in urban environments. A medium without any jamming issues seems almost impossible to exist in today's warfare. Basically, noise jamming issues were taken into consideration. *Urbana* Wireless Toolset was used as the computer simulation. Even though it is a powerful tool to predict the radio wave propagation in urban environments, due to the problems about modeling the cities (lack of detail, like the shapes of the buildings, objects and vehicles that could be found in the streets, and other details that would contribute to the propagation mechanisms), it can only give us a trend with some guidelines instead of an exact mapping of propagation.			
14. SUBJECT TERMS Unmanned aerial vehicles relay, Communication jamming, Urban propagation, *Urbana* wireless toolset, Antennas in communication systems.			**15. NUMBER OF PAGES** 103
			16. PRICE CODE
17. SECURITY CLASSIFICATION OF REPORT Unclassified	**18. SECURITY CLASSIFICATION OF THIS PAGE** Unclassified	**19. SECURITY CLASSIFICATION OF ABSTRACT** Unclassified	**20. LIMITATION OF ABSTRACT** UL

NSN 7540-01-280-5500 Standard Form 298 (Rev. 2-89)
Prescribed by ANSI Std. 239-18

THIS PAGE INTENTIONALLY LEFT BLANK

Approved for public release, distribution is unlimited

FREQUENCY AND POLARIZATION DIVERSITY JAMMING OF COMMUNICATIONS IN URBAN ENVIRONMENTS

Tuncay Ulama
1st Lieutenant, Turkish Army
B.S., Turkish Army Academy, 1999

Submitted in partial fulfillment of the
requirements for the degree of

MASTER OF SCIENCE IN SYSTEMS ENGINEERING

from the

NAVAL POSTGRADUATE SCHOOL
September 2005

Author: Tuncay Ulama

Approved by: David C. Jenn
Thesis Advisor

Daniel C. Schleher
Second Reader

Dan Boger
Chairman, Department of Information Sciences

THIS PAGE INTENTIONALLY LEFT BLANK

ABSTRACT

The purpose of this research is to investigate how to exploit frequency and polarization techniques in reducing the effects of jamming against UAV relay communication links in an urban warfare environment. There have been early studies investigating the diversity techniques against multipath and fading problems in urban environments. A medium without any jamming issues seems almost impossible to exist in today's warfare. Basically, noise jamming issues were taken into consideration. *Urbana* Wireless Toolset was used as the computer simulation. Even though it is a powerful tool to predict the radio wave propagation in urban environments, due to the problems about modeling the cities (lack of detail, like the shapes of the buildings, objects and vehicles that could be found in the streets, and other details that would contribute to the propagation mechanisms), it can only give us a trend with some guidelines instead of an exact mapping of propagation.

THIS PAGE INTENTIONALLY LEFT BLANK

TABLE OF CONTENTS

LIST OF FIGURES

LIST OF TABLES

THIS PAGE INTENTIONALLY LEFT BLANK

ACKNOWLEDGMENTS

I would like to extend my sincere thanks to my thesis advisor, Professor David C. Jenn, Naval Postgraduate School, Monterey, CA, for his patience, guidance, and flexibility throughout the thesis process. I also would also like to thank Professor Daniel C. Schleher for his valuable advice and support as the second reader. I am most grateful to my wife, Meltem, for her endless love, support, encouragement, and understanding in completing my Master's Degree and this thesis. Additionally, I would like to thank my parents for their continuing love and support. Everything that I have accomplished in my life is a direct result of their dedication and belief in me.

Finally, I would like to express my sincere gratitude to my country, Turkey, and to the Turkish Army for giving me the opportunity to undertake this study.

THIS PAGE INTENTIONALLY LEFT BLANK

I. INTRODUCTION

A. COMMUNICATION ISSUES IN MILITARY OPERATIONS ON URBANIZED TERRAIN (MOUT)

Military urban operations can probably be considered the most difficult type of operation that ground forces of any military must perform today. Both the physical characteristics of urban terrain and the presence of civilians can prohibit or limit the effectiveness of firepower provided by tanks, artillery and airpower. Communications also becomes a concern at the lowest tactical levels, where infantrymen must fight and coordinate with each other while moving through back alleys and buildings. These structures impede command, control and communications (C3) since they interfere with the transmitted signals. They absorb, reflect or block the signals. The communication problem also includes the growing demand for information by the war fighters. Models and simulations have shown that when soldiers are connected to a communication network, combat effectiveness is increased, resulting in higher lethality and lower causalities [1]. As an example, the U.S. Army is 'digitizing' all army field units by applying digital information technologies to meet such a demand [2].

Urban terrain presents huge communication problems since the power constraints associated with man-portable radios, fading, path loss and Non-Line of Sight (NLOS) situations. First, man-portable radios present tradeoffs. The main tradeoff is that while higher frequencies can support higher information rates, they often require more power to avoid getting blocked, larger antennas, and more expensive equipment. This is why it is difficult to build man-portable radios capable of high enough data transfer for video transmissions. Second, fading occurs because of multipath propagation. It refers to a temporal variation in received signal strength. Multipath propagation results from the reflecting objects and scatterers such as buildings, vehicles, street lampposts, and traffic lights. When direct and reflected waves from the same signal arrive at the receiver along different paths with different phases, they are thus subjected to destructive interference, and fading occurs. Third, path loss also occurs when radio signals are attenuated as they pass through walls, buildings and other obstacles in the path. Signal energy is absorbed or reflected as it hits different objects. Fading and path loss are illustrated in Figure 1.

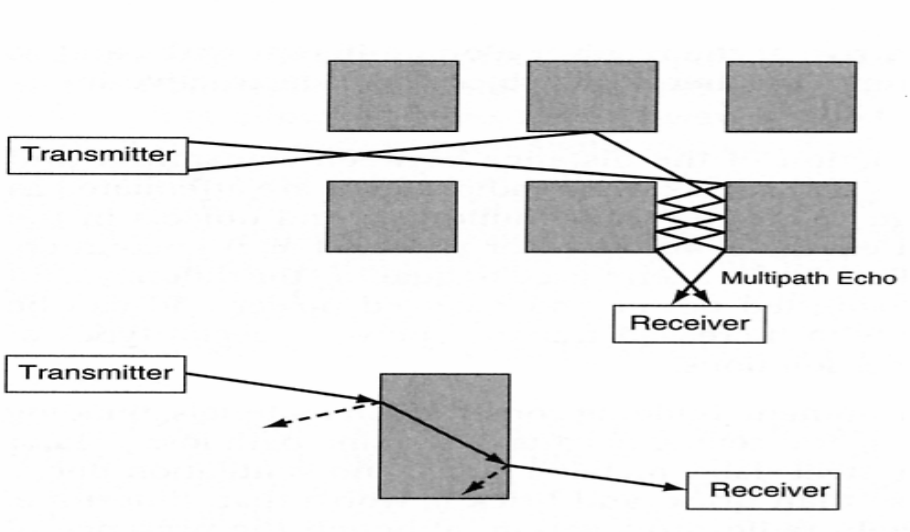

Figure 1. Fading (above) and Path Loss (below) (From Ref. [3]).

Last, but not least, since the mobile land forces fighting in MOUT are usually dispersed, they are confronted with NLOS situations. Adding a relay can establish a communication link between a receiver and a transmitter that are not in line of sight with each other. In the past, the common practice was to establish ground-base relay sites. Today, the relay concept could be extended to Unmanned Aerial Vehicles (UAVs) since the technology is available.

B. UNMANNED AERIAL VEHICLES (UAV) AS COMMUNICATION RELAYS

Unmanned Aerial Vehicles (UAVs) have also been referred to as Remotely Piloted Vehicles (RPVs), drones, robot planes, and pilot-less aircraft. UAVs are either described as a single air vehicle (with associated surveillance sensors), or a UAV system, which usually consists of three to six air vehicles, a ground control station, and accompanying support equipment [4]. The military effectiveness of UAVs in recent conflicts such as Iraq (2003), Afghanistan (2001), and Kosovo (1999) has shown the advantages and disadvantages they provided. They can be used as an alternative to manned aircraft in three-dimensional (3-D) missions; those dull, dirty or dangerous missions that do not require a pilot in the cockpit.

UAVs have recently been given a higher priority since technology is now available that was not available just a few years ago. There are various applications in which UAVs are used. Predator, which is one of the major UAVs flown by the U.S.

military today, hit Taliban and Al Qaeda leaders in Afghanistan and Yemen with Hellfire missiles. In the future, they could take on the aerial refueling task now performed by KC-10 and KC-135 tanker aircraft. However, UAVs have traditionally been used as Intelligence, Surveillance and Reconnaissance/Target Acquisition (ISR/TA) assets. They provide commanders with imagery intelligence, electronic intelligence, and streaming video. This information can be used to direct fighter aircraft to their targets, to monitor enemy troop movements and to conduct battle damage assessment.

As communications in MOUT become an issue, UAVs can effectively be used as communication relays in these operations. Adding a relay can establish a communication link between a receiver and a transmitter that are not in line of sight with each other. UAV relays can shorten the link distance and overcome noise and Line of Sight (LOS) problems for units positioned in cities. The Israeli Defense Force (IDF) pioneered the use of RPVs for radio relay platforms and used them to provide real-time battlefield updates to commanders [3].

The U.S. Marine Corps also evaluated UAVs to see if they could serve as relays for a Marine tactical radio. It was found that smaller, tactical UAVs should be considered. Any tactical UAV capable of carrying more than 25 pounds could possibly serve as a communication relay [3]. The UAVs evaluated include Dragon Eye and Dragon Warrior. They provide over-the-hill reconnaissance, surveillance, and target acquisition at the tactical level. Dragon Eye has a wingspan of just 45 inches; it can be stored in a backpack and launched either by hand or bungee cord. These capabilities make it very useful in an urban warfare environment. Dragon Warrior is also a low-cost vertical takeoff and landing (VTOL) drone. Like Dragon Eye, it is envisioned to play a major role in cities. These UAVs are illustrated in Figure 2.

Figure 2. Dragon Eye (Left) and Dragon Warrior (Right) (From Ref. [4]).

C. COMMNICATIONS JAMMING

The communication issues mentioned in Section A of this Chapter arise using communications equipment in and near buildings and structures in a city. There are additional issues presented when friendly forces operate in an urban environment. Radio links are the prime target for Electronic Attack (EA). They have been exploited in several recent conflicts. They have been jammed and their data intercepted [5]. Voice, data, and even missile-command links are vulnerable to jamming. If the operation is disrupted, the result can be chaos, which an enemy can exploit quickly.

The history of modern war is full of successful examples of jamming communication links. During the Beka's Valley air battles, Israeli Defense Force Air Force (IDF-AF) aircraft jammed Syrian surface-to-air communication links, which deprived Syrian Air Force fighters of ground control. That resulted in an 80 to 2 score which the Israelis claimed in air-to-air combat during the first week of the campaign [6].

Basic communication jammers act as noise generators. The output of the jammer transmitter can be spread over the entire range of frequencies used by the enemy. This is called "barrage noise jamming." It requires considerably more Effective Radiated Power (ERP) for a jammer, so it is difficult to achieve. Alternatively, power can be selectively focused on a few key transmissions, which is a technique called "spot jamming." It is used when the frequency parameters (center frequency and bandwidth) of the victim system to be jammed are known. Spot jamming is most effective since it concentrates the effect of the jamming. It requires less ERP and leaves most of the frequency band unjammed, and thus free for friendly communications [6].

It should always be taken into consideration that the data links between ground units fighting in cities and UAV relays flying over them are potentially subject to jamming by the enemy.

D. OBJECTIVE

For military urban operations, secure reliable communication becomes a concern at the lowest tactical levels, where infantrymen must fight and coordinate with each other while moving between and through buildings. Since the mobile land forces fighting in MOUT are usually dispersed, they are confronted with NLOS situations. Adding an airborne relay can establish a communication link between a receiver and a transmitter that are not in line of sight of each other. With the technology available, UAVs can be used as relays. Radio links used by these types of relays would be the prime target for EA in an urban warfare environment. The enemy could use noise generators to jam the links.

The purpose of this research is to investigate how jammer signals behave in an urban environment and how to exploit diversity techniques in mitigating the effects of jammers. The focus is to seek improvement on the performance of UAV relays data links in the presence of jamming. The techniques to be explored are polarization and frequency diversities. This research first addresses the background information on jamming theory, antennas, and propagation principles. Then it involves modeling, simulation, and analysis of the UAV relay data link performance in the presence of a noise jammer. The modeling and simulation provides insight into the characteristics of urban radiowave propagation and effectiveness of diversity techniques on the link performance when being jammed. The ultimate goal of this research is to recommend possible guidelines for operating UAV relays for MOUT.

E. THESIS OUTLINE

Chapter II discusses communications Electronic Protection (EP) techniques used in military operations, calculation of signal-to-jam ratio (S / J), and the role of antennas in communication systems. Discussions of the antenna performance parameters, thin-wire dipoles and the Friis transmission equation are included in the communication systems section.

Chapter III discusses some of the important relevant propagation mechanisms and both theoretical and empirical models that are used for urban propagation. The *Urbana*

Wireless Toolset is also described. It is a powerful computational electromagnetic tool for simulating wireless propagation in complex environments such as cities.

Chapter IV presents the simulations and analyzes the results. Chapter V summarizes the results and makes suggestions for future work. Finally, Appendix A shows a sample *Urbana* input script that was used in the simulations and Appendix B lists the *Matlab* codes used in this thesis.

II. JAMMING THEORY AND ANTENNAS IN COMMUNICATION SYSTEMS

In this Chapter, communications Electronic Protection (EP) techniques used in military systems, calculation of signal-to-jam ratio (S/J), and the role of antennas in communication systems will be discussed. The main EP techniques used today can be broken into in three categories. They are:

- Spread Spectrum (waveform design)
- Error-Control Coding
- Antenna techniques.

The emphasis will be on antennas since the simulations will be dealing with the antenna parameters in communication systems and jammers. Furthermore, the antenna techniques can be applied in addition to the first two.

The ratio of the desired signal power to the jammer signal power is the signal-to-jam ratio (S/J). It gives the information necessary to evaluate the link availability when jamming occurs.

A discussion about the antenna performance parameters is important since every electronic-warfare system that either radiates or receives electromagnetic energy from the atmosphere must involve an antenna. At the end of the Chapter, the Friis Transmission Equation, also known as the Link Equation, is studied. The model used in the simulations includes a transmitter antenna and an observation plane that may be considered as the location of receiver antennas. The Friis Transmission Equation relates the power received to the power transmitted between two antennas separated in space.

A. COMMUNICATIONS ELECTRONIC PROTECTION (EP) TECHNIQUES

In today's modern military strategy, communication systems have very important roles such as providing the means for command and control between the commanders and their units, and allowing transmission of battlefield information to all forces. In the past, the strategy was superiority in numbers, but now it has become how efficiently forces can share information and intelligence. This is not as easy in practice as it might seem. There are three major aspects of the problem. They are Electronic Support (ES),

Electronic Attack (EA) and Electronic Protection (EP). ES involves actions to search, intercept, identify and locate sources of intentional and unintentional radiated electromagnetic energy. EA involves the use of electromagnetic or directed energy to attack personnel, facilities or equipment. The aim is to degrade, neutralize or destroy the enemy's combat capability. Finally, EP involves actions taken to protect friendly personnel, facilities and equipment from those types of effects described in EA. [7]

The operation of communication and data links is more complex in urban environments than conventional battlefields, such as open terrain or fields with some low vegetation. In cities, the electromagnetic wave propagation has a complex behavior that is a combination of direct, reflected, and diffracted signal components. When jamming issues are added to this scenario it becomes even more complicated. In the city, the enemy would want to use EA against communication and data networks. In this case, the jamming target is the link between the UAV and friendly ground units. The primary objective is to limit situational awareness provided by a UAV by restricting the information transfer to the ground units. If a UAV is used for commanding the units by a remotely stationed commander deployed elsewhere, jamming also serves to separate the commander from his forces.

Jamming could be simply injecting noise into the communication system, as well as corrupting information in the network. The EP principles against these types of EA techniques would include [7]:

- Use of fiber optic channels to prevent interception and injection of signal.
- Use of highly directive antennas (low sidelobes will prevent detection and jamming).
- Use of anti-jam waveforms in time, frequency and coding domains.
- Use of encryption.

The EP techniques used in military systems are illustrated in Figure 3.

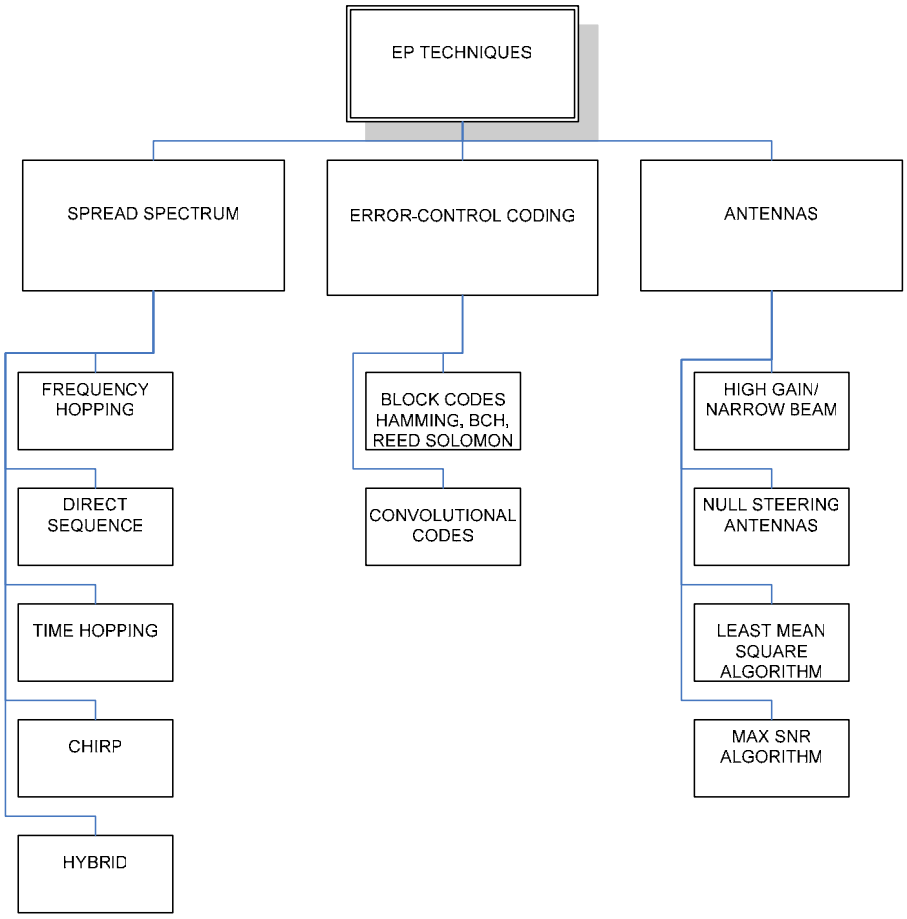

Figure 3. Communications EP Techniques (From Ref. [7]).

In this thesis, there is special emphasis on the antenna and its role in both the communication system and jammer. First, the antennas that have high gains and narrow beams can provide EP using their spatial filtering ability. In the microwave region (1 GHz – 100 GHz), highly directive antennas that are useful for point-to-point communication systems can be designed.

A second technique for jammers located at angles displaced from the axis of the main antenna beam is to employ low-sidelobe technology. Sidelobe cancellation systems are used with directive antennas. They provide additional attenuation of sidelobe jammers. In these systems, the "guard antennas" are used to generate antenna patterns that provide nulls in the direction of jammer. In theory, the number of sidelobe jammers that can be nulled is equal to the number of auxiliary antennas. [7]

Third, the least mean-square adaptive algorithm can be used as a method in which the reference signal is equal to the desired response of the antenna system. The algorithm updates the new equalizer weights based on the existing weights and a factor depending on the current input samples and the current estimation error. The weights are selected to minimize the mean-square value of the error signal caused by the jammer. The error signal is the difference between antenna output and the reference signal.

The last approach illustrated in Figure 3 is the maximum SNR algorithm. If we use an appropriately defined SNR, F , then we can find the optimum set of weights for the individual antennas in order to maximize the ratio. An antenna system based on these weights produce $K-1$ nulls (with K antenna elements) directed toward $K-1$ interfering transmitters sufficiently spaced apart. [8]

B. SIGNAL-TO-JAM RATIO (S/J)

The injection of noise into the communications receiver is one of the basic techniques in EA. The ratio of the desired signal power to the jammer signal power is the signal-to-jam ratio (S/J). For the link to be effective, S usually should exceed J by some significant amount. The term S/J may sometimes be confusing. The effectiveness of Electronic Protection (EP) is not a direct mathematical function of S/J . The magnitude of S/J required for effectiveness is a function of a particular EP technique. It means that different techniques may require different S/J ratios against the same jammer. If there is sufficient S/J for link effectiveness, increasing it will rarely increase the effectiveness at a given range.

The S/J for noise jamming is: [7]

$$\frac{S}{J}=\frac{P_t G_{tr} G_{rt} R^2{}_{jr} L_j B_j}{P_j G_{jr} G_{rj} R_{tr}{}^2 L_r B_r}\left|F\right|^2 \tag{2.1}$$

where

P_j = jammer power

P_t = communication transmitter power in the direction of the communication receiver

G_{jr} = antenna gain of the jammer in the direction of the communication receiver

G_{rj} = antenna gain of the communication receiver in the direction of the jammer

G_{rt} = antenna gain of the communication receiver in the direction of the communication transmitter

G_{tr} = antenna gain of the communication transmitter in the direction of the communication receiver

B_r = communications receiver bandwidth

B_j = jamming transmitter bandwith

R_{tr} = range between communications transmitter and receiver

R_{jr} = range between jammer and communication receiver

L_j = jammer signal loss (including polarization mismatch)

L_r = communication signal loss

F = path gain factor.

Generally, S/J ratios less than about 10 dB can cause serious interference problems. Equation (2.1) can also be used to solve for the effective radiated power (ERP) which is the jamming power or the maximum range at which the jamming is effective.

C. ANTENNAS IN COMMUNICATIONS SYSTEMS

Communication links are the main application area for antennas. A communication link simply consists of a transmitter and a receiver separated by a distance R. The total power incident on the receiver antenna can be found by summing up the incident power density over the effective aperture (A_e). Effective aperture (also called effective area) is related to the physical area A by $A_e = eA$, where e is the aperture efficiency. How an antenna converts the incident power into available power depends upon the type of the antenna, the direction it is pointing, and polarization [7].

1. Description of Antenna Performance Parameters

With regard to communications and jamming, the relevant antenna parameters of concern are:

- Directivity
- Gain
- Polarization
- Input impedance

- Radiation pattern
- Bandwidth.

These aspects of antenna are discussed briefly in this section.

The *radiation pattern* gives the angular variation of radiation at a fixed distance from an antenna when the antenna is transmitting [1]. Radiation is quantified by noting the value of power density at a fixed distance R from the antenna. By reciprocity, a receiving antenna comprised of linear reciprocal components responds to an incoming wave from a given direction according to the transmit pattern value in that direction (i.e., the transmitting and receiving patterns are identical) [9].

Radiation patterns can be understood by examining the ideal dipole. In Figure 4 (a), we see the fields radiated from an ideal dipole over the surface of a sphere of radius r in the far field. In the far field, the outgoing wave front is spherical and only the transverse field components are significant.

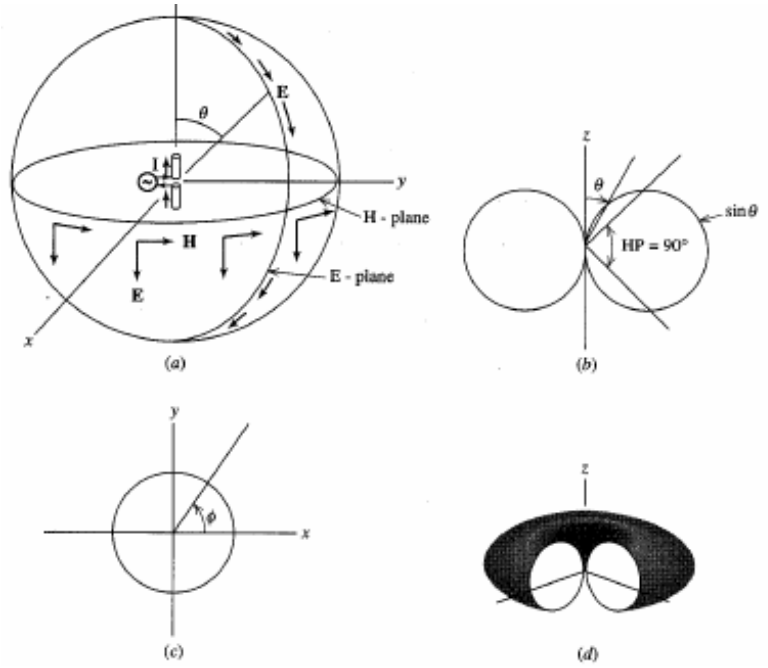

Figure 4. Radiation from an ideal dipole. (a) Field components. (b) E-plane radiation pattern polar of $|E_\theta|$ or $|H_\phi|$. (c) H-plane radiation pattern polar plot of the $|E_\theta|$ or $|H_\phi|$. (d) Three-dimensional plot of radiation pattern. (From Ref. [1]).

The field vectors are shown at an instant of time for which the fields are at a maximum. The angular variation of E_θ and H_θ over the sphere is $\sin\theta$. Any plane containing the z-axis has the same radiation pattern since there is no ϕ variation in the fields. A pattern taken in one of these planes is called an *E-plane pattern* since it contains the electric field vector. A pattern taken in a plane perpendicular to an E-plane and cutting through the test antenna (the *xy*-plane in this case) is called an *H-plane pattern* since it contains the magnetic field H_ϕ. These two patterns are called *principal plane patterns*; Figures 4 (b) and 4 (c) show these patterns. These are polar plots, for which the distance from the origin to the curve is proportional to the field intensity. Finally, we see the three-dimensional plot of radiation in Figure 4 (d). For the ideal dipole, this is a solid surface that resembles a "doughnut" with no hole.

Directivity is the ratio of power density in the direction of the pattern maximum to the average power density at the same distance from the antenna. It expresses how much greater the peak radiated power density is for an antenna than it would be if all the radiated power were distributed uniformly around the antenna.

$$D(\theta,\phi) = \frac{U(\theta,\phi)}{U_{\text{ave}}} \tag{2.2}$$

U is the radiation intensity (watts per steradian). If we divide the numerator and denominator by r^2, then we have power densities. So, directivity is also the ratio of the power density in a certain direction at a given range r to the average power density at that range. Mathematically:

$$G = eD_0\ D(\theta,\phi) = \frac{U(\theta,\phi)/r^2}{U_{\text{ave}}/r^2} = \frac{1/2\,\text{Re}\left(\vec{E}\times\vec{H}^*\right)\hat{r}}{P_{\text{rad}}/4\pi r^2} \tag{2.3}$$

where P_{rad} is the total radiated power and Re is the real operator.

Substitution of the formula for average power for U_{ave} in (2.2) yields

$$U_{\text{ave}} = \frac{1}{4\pi}\iint U(\theta,\phi)\, d\Omega = \frac{P}{4\pi} \tag{2.4}$$

$$D(\theta,\phi) = \frac{4\pi}{\Omega_A}\left|F(\theta,\phi)\right|^2 \tag{2.5}$$

where Ω_A is the beam solid angle which is defined by

$$\Omega_A = \iint \left|F(\theta,\phi)\right|^2 d\Omega \tag{2.6}$$

and $F(\theta,\phi)$ is the normalized field pattern

$$\left|F(\theta,\phi)\right| = \frac{\left|E_\theta\right|}{\left|E_\theta\right|_{\max}}. \tag{2.7}$$

When directivity is mentioned as a single number without reference to a direction, maximum (peak) directivity is usually intended. The directivity is the maximum value of the directive gain [10].

$$D_0 = D_{\max}(\theta,\phi) = D(\theta_{\max},\phi_{\max}) \tag{2.8}$$

This is illustrated in Figure 5. If the radiated power were distributed isotropically over all of the space then $U_m = U_{\text{ave}}$, which means the radiation intensity would have a maximum value equal to its average value, as shown in Figure 5 (a). The beam solid angle is $\Omega_A = 4\pi$. Here, the directivity of this isotropic pattern is unity. For an actual antenna, the distribution of radiation intensity $U(\theta,\phi)$ is illustrated in Figure 5 (b). It has maximum radiation intensity in the direction $(\theta_{\max},\phi_{\max})$ of $U_m = DU_{\text{ave}}$ and an average radiation intensity of $U_{\text{ave}} = P_{\text{rad}} / 4\pi$.

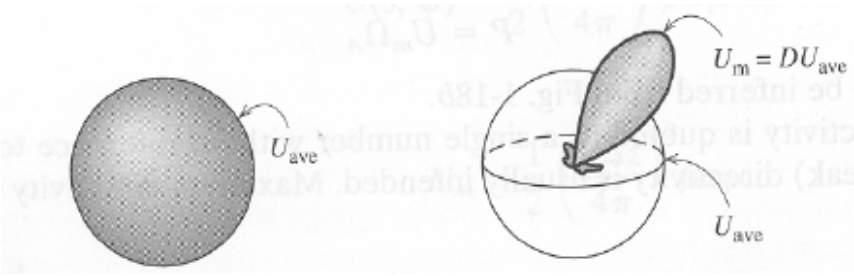

Figure 5. Illustration of directivity. (a) Radiation Intensity Distributed Isotropically. (b) Radiation Intensity from an Actual Antenna (From Ref. [9]).

Gain is the directivity reduced by the losses of the antenna [9]. Directivity is only determined by the radiation pattern of an antenna. Gain (sometimes called power gain) is defined as 4π times the ratio of the radiation intensity in a given direction to the net power accepted by the antenna:

$$G(\theta,\phi) = \frac{4\pi U(\theta,\phi)}{P_{\text{in}}} = eD \tag{2.9}$$

where e is the antenna efficiency. This formula includes the effect of any losses on the antenna but does not include the losses due to mismatches of impedance or polarization. The maximum gain is

$$G = eD_0 \tag{2.10}$$

If no direction is defined, then the formula above is used, and the gain is assumed to be the maximum gain.

Here, we should notice a significant difference between the reference power used to define directivity and gain. The formula used for directivity is relative to the radiated power, whereas gain is defined with respect to input power. Gain includes the fact that some of the input power is lost in the antenna. The lost portion of P_{in} is absorbed in the antenna in the form of ohmic, dielectric, or mismatch loss.

Polarization describes the vector nature of electric fields radiated by an antenna. The polarization of an antenna is the polarization of the wave radiated in a given direction by the antenna when transmitting [9]. Usually, the polarization characteristics of an antenna remain relatively constant over its main beam and the polarization on the main beam peak is used to describe the antenna polarization. However, we cannot skip the measurements of the sidelobes. The radiation from sidelobes can differ greatly in polarization from that of the main beam. One should measure E_θ and E_ϕ to characterize the antenna's polarization.

At a fixed point in space, the tip of the E-field vector traces out a path that determines the polarization. A straight wire antenna radiates a wave with linear polarization parallel to the wire. Another common polarization is circular. The most general case is elliptical, in which both field components present with arbitrary amplitude and phase relationship. The general polarization ellipse is illustrated in Figure 6.

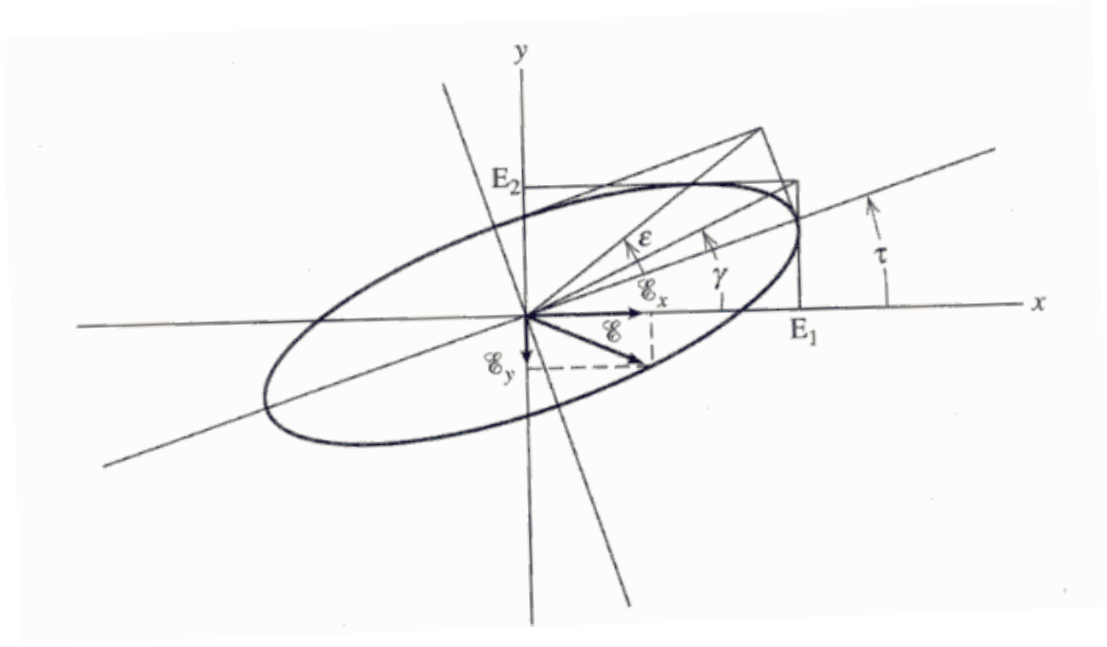

Figure 6. The general polarization ellipse. The wave direction is out of the page in the + z direction. The tip of the instantaneous electric vector $\mathscr{E}$ traces out the ellipse (From Ref. [9]).

The sense of rotation may be either left or right. As illustrated in Figure 7, the instantaneous electric field vector $\mathscr{E}$ has components $\mathscr{E}_x$ and $\mathscr{E}_y$ along the x- and y-axis. The peak values of the components are E_1 and E_2 and

$$\gamma = \tan^{-1}\frac{E_2}{E_1}, \qquad 0^o \le \gamma \le 90^o \tag{2.11}$$

τ is the tilt angle of the ellipse. It is the angle between the x-axis (horizontal) and the major axis of the ellipse. As to the angle ε,

$$\varepsilon = \cot^{-1}(-AR), \qquad 1 \le |AR| \le \infty, \qquad -45^o \le \varepsilon \le 45^o \tag{2.12}$$

where $|AR|$ is the axial ratio; that is, the ratio of the major axis electric field component to that along the minor axis. The sign of AR is positive for right-hand sense and negative for left-hand sense.

The *input impedance* (Z_A) of an antenna is the ratio of the voltage to current at the antenna terminals. The antenna input impedance should be matched to the characteristic impedance of the connecting transmission line to minimize mismatch loss. The input impedance may be affected by other antennas or objects that are nearby. Here, this effect is ignored (it is assumed that antenna is isolated).

Input impedance has real and imaginary parts:

$$Z_A = R_A + jX_A = R_L + R_r + jX_A \tag{2.13}$$

where R_A is input resistance which represents power delivered to one of two loads. One is free space, represented by the load R_r, and the other is ohmic or other loss, R_L. The reactance X_A represents power stored in the near field of the antenna. Normally, for a

resonant antenna, X_A should be nearly zero over the operating band. The impedance of an antenna is usually identical for reception and transmission due to reciprocity.

Bandwidth is defined as "the range of frequencies over which important performance parameters is acceptable" [9] or "the range of frequencies within which the performance of the antenna, with respect to some characteristics, conforms to a specified standard" [11]. The characteristics referred to are pattern, input impedance, beamwidth, polarization, gain, radiation efficiency, and so forth.

The bandwith for broadband antennas, such as spiral and log periodic dipole arrays which have low to moderate gain, constant gain, and real input impedance, is usually expressed as the ratio of the upper-to-lower frequencies of acceptable operation. f_L and f_H, respectively. A 10:1 bandwidth means the upper frequency is 10 times greater than the lower frequency. The percentage bandwidth is

$$\frac{f_H - f_L}{f_c} \times 100 \tag{2.14}$$

and

$$f_c = \frac{1}{2}\left(f_H + f_L \right) \tag{2.15}$$

where f_c is the center frequency. As an example, when we say 10% bandwith, the frequency difference of acceptable operation is 10% of the center frequency of the bandwith [11].

2. Thin-wire Dipoles

The half-wave dipole antenna is a very widely used antenna in communication systems, and the simulations performed later in this thesis employ this type of antenna. It is basically a linear current whose amplitude varies as one-half of a sine wave with a maximum at the center [9]. The advantage of a half-wave dipole is that it can be made to resonate and present a zero input reactance ($X_A = 0$). This helps to eliminate the need for tuning to achieve a conjugate impedance match. To obtain a resonant condition for a half-wave dipole, the physical length must be somewhat shorter than a free space half-wavelength. As the antenna wire thickness is increased, the length must be reduced more

to achieve resonance [9]. The patterns for half-wave dipole are illustrated in Figure 7. The complete (normalized) far-field pattern of a half wave dipole is

$$F(\theta) = \frac{\cos\left[(\pi/2)\cos\theta\right]}{\sin\theta}. \tag{2.16}$$

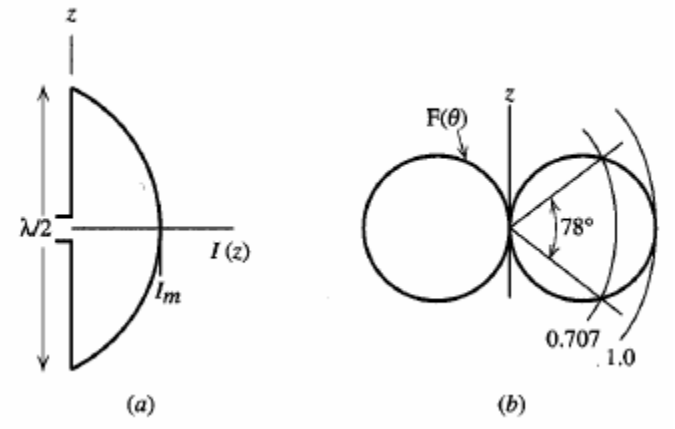

Figure 7. The half-wave dipole. (a) Current Distribution, $I(z)$ (b) Radiation Pattern $F(\theta)$ (From Ref. [1]).

3. Friis Transmission Equation

The Friis Transmission Equation (also referred to as the link equation) relates the power received to the power transmitted between two antennas separated by a distance R. A typical geometrical orientation of transmitting and receiving antennas is shown in Figure 8.

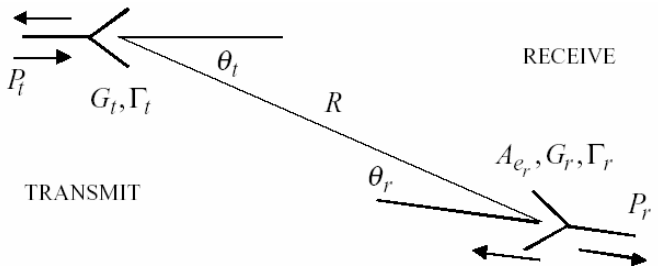

Figure 8. Geometrical orientation of transmitting and receiving antennas.

If the input power at the terminals of the transmitting antenna is P_t, then the power density at range R in the direction θ_t, ϕ_t is

$$W_t(\theta,\phi) = \frac{P_t G_t(\theta_t,\phi_t)}{4\pi R^2} \tag{2.17}$$

where $G_t(\theta_t,\phi_t)$ is the gain of the antenna in the direction θ_t, ϕ_t. The effective aperture A_e of the antenna is related to its gain by

$$A_e = G(\theta_r,\phi_r)\left(\frac{\lambda^2}{4\pi}\right). \tag{2.18}$$

The amount of power P_r collected by the receiving antenna can be written, using Equations (2.20) and (2.21) and the polarization loss factor, as

$$P_r = e_t D(\theta_t,\phi_t)\frac{\lambda^2}{4\pi}W_t = \frac{\lambda^2 G(\theta_t,\phi_t)G(\theta_r,\phi_r)P_t}{(4\pi R)^2}\left|\hat{\rho}_t.\hat{\rho}_r^{\,*}\right|^2 |F|^2 \tag{2.19}$$

or

$$\frac{P_r}{P_t} = \left(1-|\Gamma_t|^2\right)\left(1-|\Gamma_r|^2\right)\left(\frac{\lambda}{4\pi R}\right)^2 G(\theta_t,\phi_t)G(\theta_r,\phi_r)\left|\hat{\rho}_t\hat{\rho}_r^{\,*}\right|^2 |F|^2 \tag{2.20}$$

where Γ_t is the transmitter antenna input reflection coefficient, and Γ_r is the receiver antenna input reflection coefficient, $\hat{\rho}_t$ is the unit vector of transmitter antenna, $\hat{\rho}_r$ is the unit vector of receiver antenna, and $|F|$ is the path gain factor calculated by *Urbana*.

Finally, one can write this equation for input matched and polarization matched antennas (aligned for maximum directional radiation and reception) as:

$$\frac{P_r}{P_t} = \left(\frac{\lambda}{4\pi R} \right)^2 G_t G_r \left| F \right|^2 . \tag{2.21}$$

Equations (2.20) and (2.21) are known as the *Friis Transmission Equation*. It relates the power P_r (delivered to the receiver load) to the input power of the transmitting antenna P_t. The term $\left(\lambda / 4\pi R\right)^2$ is called the *free-space loss factor*, and it takes into account the losses due to the spherical spreading of energy [11].

D. SUMMARY

In this chapter, communications Electronic Protection (EP) techniques used in military systems, signal-to-jam ratio (S/J), and antennas in communication systems were discussed. The main communications EP techniques are spread spectrum, error-control coding, and antennas. Spread-spectrum techniques and error-control coding were not discussed in this study. The emphasis was on the antenna and its role in the communication system and jammer. Antennas that have high gains, narrow beams, null steering antennas, the least mean square adaptive algorithm, and maximum SNR algorithm are among the antenna EP techniques. Since the emphasis was on antennas, some of the important antenna performance parameters were explained. Thin-wire dipoles and the Friis Transmission Equation were also mentioned.

In the next chapter, both theoretical and empirical models that have been used to predict signal levels in an urban environment are studied. The *Urbana* Wireless Toolset is also mentioned as a computational electromagnetic tool for simulating wireless propagation in complex environments.

THIS PAGE INTENTIONALLY LEFT BLANK

III. URBAN PROPAGATION AND URBANA WIRELESS TOOLSET

In the first part of this Chapter, some of the important relevant propagation mechanisms and both theoretical and empirical models that predict urban propagation will be discussed. It is necessary to have a basic knowledge about the propagation mechanisms to understand the radio wave propagation in urban environments. Propagation of radio waves is strongly influenced by them.

In the second part, the *Urbana* Wireless Toolset is studied. It is a powerful computational electromagnetic tool for simulating wireless propagation in complex environments. Today, propagation modeling is used for different applications such as mobile communications systems, wireless local area networks, GPS performance evaluation, and data links for UAVs.

A. URBAN PROPAGATION

1. Introduction

Even though urban environments are encountered in many military and commercial applications, modeling and simulation of urban propagation is a relatively new area of study. It is essential to predict the characteristics and mechanisms of propagation in order to be able to adequately design communication devices and systems. The mechanisms are basically grouped into *reflection, diffraction, scattering* and *absorption.*

When a propagating electromagnetic wave hits a reflecting surface and that surface has very large dimensions compared to the wavelength of the signal, then specular reflection occurs. Snell's Law predicts the angle of reflection based on the angle of incidence. *Reflection* may occur from the building walls and windows, obstacles in the street and from the surface of the earth when the ground is flat compared to the wavelength.

If an obstacle with an edge (i.e. building) is sitting in the communication path between the transmitter and receiver, then *diffraction* occurs due to the knife-edges and

corners of the obstacle. A diffracted wave can account for the maintenance of the communication channel when a LOS path does not exist.

In the cases in which there are objects with small dimensions compared to the wavelength in the path of the wave, *scattering* occurs. Even dust particles or raindrops can contribute propagation by behaving like isotropic scatterers. They scatter the energy uniformly in all directions. Larger objects than these, such as tree leaves, can also contribute to scattering.

While the waves are propagating through a lossy medium such as a wall or even a cloud, they are attenuated. *Absorption* refers to energy dissipation inside of these materials or media. The attenuation constant is dependent upon the material's permittivity, permeability and conductivity. The propagation mechanisms summarized above are illustrated in Figure 9.

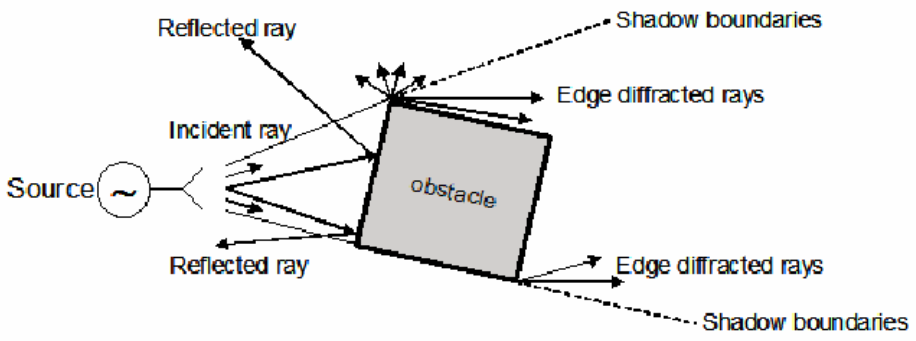

Figure 9. Propagation Mechanisms (From Ref. [12]).

Different approaches have been used to explain radio wave propagation in urban environments. There are theoretical models and empirical models for investigating urban propagation. Theoretical models start with Maxwell's equations and the boundary conditions. They are purely analytical approaches and depend upon an assumption of regularity in the urban environment. As to empirical models, they rely on curve-fitting measured radio wave propagation behavior as a function of multiple physical parameters describing the urban and suburban environment [10].

2. Theoretical Models of Urban Propagation

The models in this category rely on physical generalizations that allow the solution of a far simpler problem to be effectively applied to more complicated urban geometry. A theoretical solution often does not give us practical results since the oversimplified assumptions of the geometry for such problems may not be good in real life. The urban problem is more complicated because the fields in the immediate vicinity of the portable or mobile radio are a superposition of localized multipath scattering [10]. However, theoretical models help in understanding the phenomenology of scattering. Some simple models are discussed in the following section.

a. The Diffracting Screens Model

The model by Walfisch and Bertoni assumes that buildings in a city have nearly uniform height (homogenous neighborhood) and are organized into rows of streets. The propagation is from a fixed-site antenna in the city to a final diffraction of the rooftop field down to a street level mobile or portable radio. This is illustrated in Figure 10.

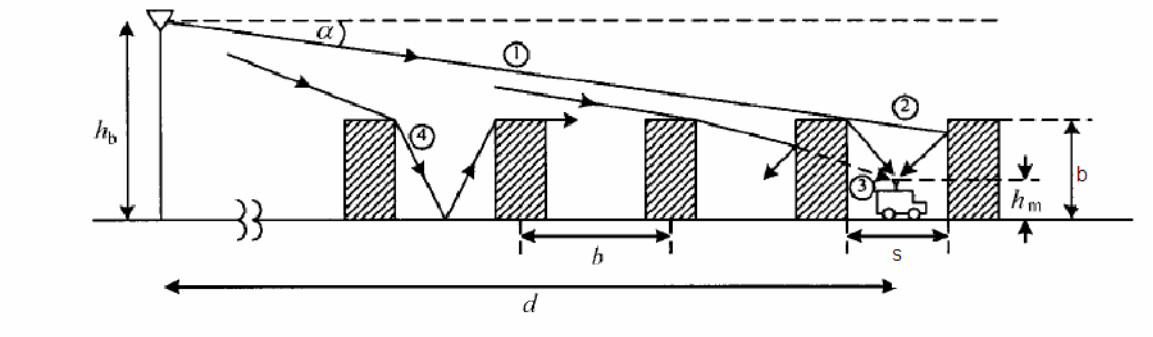

Figure 10. Wave propagation in a homogeneous urban region (After Ref. [13]).

The total signal received by the receiver is the sum of diffracted and reflected paths (ray numbers 1 and 2), multiple rooftop diffractions and reflections (ray number 4) and building penetration (ray number 3). Parameters used in the figure are:

h_b = Fixed-site antenna height, m

h_m = Mobile antenna height, m

h = Building height, m

s = Separation between rows of buildings, m.

Later, Maciel, Bertoni and Xia extended this model by allowing the fixed-site antenna to be below as well as above the rooftop level. The resulting expression for diffracting screens propagation, or average signal L_{ds} (in dB), is

$$L_{ds} = -F - L_{e1} - L_{e2} - 18\log\left[\frac{17H_b + d^2}{17H_b}\right]. \tag{3.1}$$

F is the free-space propagation loss

$$F = 32.4479 + 20\log(f_d). \tag{3.2}$$

L_{e1} is the loss for rooftop diffraction

$$L_{e1} = -10\log\left[\frac{G_m(\theta)}{\pi k\sqrt{(b - H_m)^2 + w^2}}\left[\frac{1}{\theta} - \frac{1}{2\pi + \theta}\right]^2\right]. \tag{3.3}$$

The geometry for L_{e1} is illustrated in Figure 11.

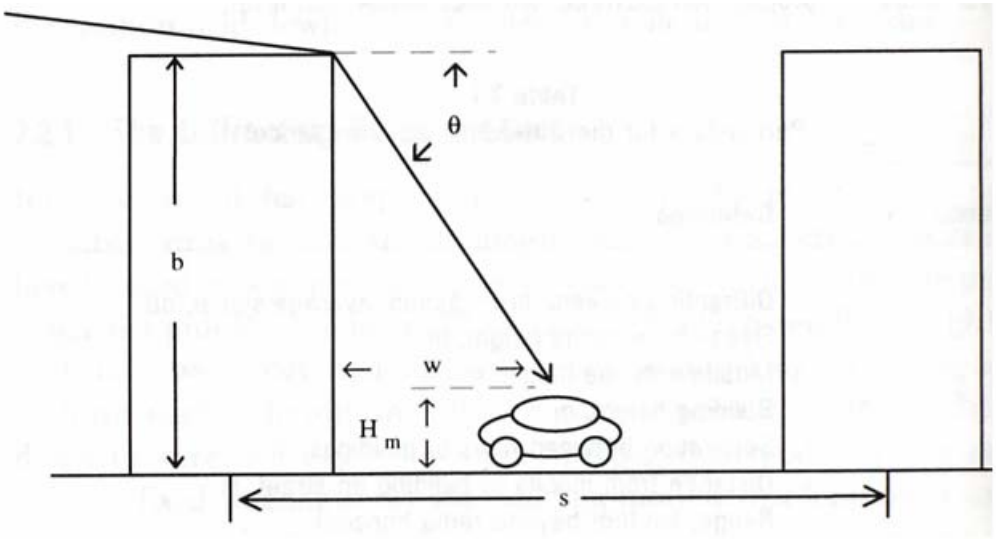

Figure 11. Local vicinity of a mobile radio in a suburban area (From Ref. [13]).

The factor L_{e2} is

$$L_{e2} = -10\log\left[G_b Q^2\right] \tag{3.4}$$

where G_b is the fixed-site antenna gain and Q is either Q_E or Q_L depending on whether the fixed-site antenna is elevated above or below the rooftop level. They are given by

$$Q_L = \frac{\frac{s}{d1,000-s}}{\sqrt{2\pi k\sqrt{\left(b-H_b\right)^2+s^2}}}\left[\frac{1}{a\tan\left[\frac{b-H_b}{s}\right]}-\frac{1}{2\pi+a\tan\left[\frac{b-H_b}{s}\right]}\right] \tag{3.5}$$

$$Q_E = 2.35\left[a\tan\left[\frac{H_b}{d1,000}\right]\sqrt{\frac{s}{\lambda}}\right]^{0.9}. \tag{3.6}$$

b. The COST 231 Model

This model, created by the European Research Committee COST 231 (evaluation of land mobile radio), was applied to the 800-1800 MHz band and tested in Germany [13]. It relies on the models of Walfisch-Bertoni and Ikegami (not included here) along with the empirical corrections. It used the results of Walfisch-Bertoni and Ikegami's correction functions to deal with street orientation. The influence of street orientation was found to be minimal after the tests.

c. Diffraction over Knife-Edge Obstacles

When there is a sharp obstacle such as fence or hill ridge high enough in the path of a propagating wave, it can obstruct the reflected ray and may also obstruct the direct ray coming from the transmitter. In this model, calculations are made by replacing the obstruction with a perfectly conducting knife-edge. The behavior of a plane wave due to the presence of a knife-edge is examined by using Huygen's principle [10].

The Huygen's principle says: Any wave front can be decomposed into a collection of point sources. New wave fronts can be constructed from the combined 'spherical wavelets' from the point sources of the old wave front. This is illustrated in Figure 12.

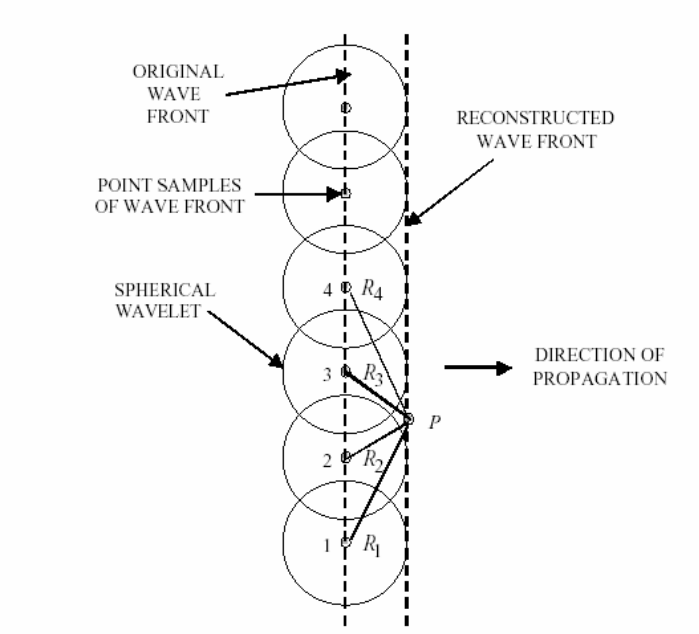

Figure 12. Huygen's principle (From Ref. [10]).

Even though a simple analytical solution exists for an infinite knife-edge, in practice it does not occur in urban environments; however, it is used to estimate diffraction loss. This model accounts for the perturbation (excess) loss for a plane wave. The edge blocks the spherical wavelets below the shadow boundary. The electric field reduces to zero for observation points deep in the shadow. This is illustrated in Figure 13.

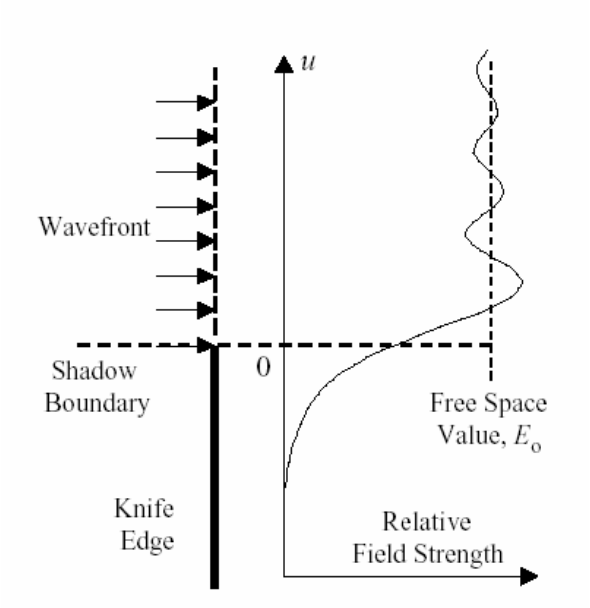

Figure 13. Knife edge E-field illustration (From Ref. [10]).

The normalized electric-field intensity (E) relative to the incident wave (E_i) is:

$$\frac{E}{E_0} = \frac{1}{2} + \frac{1+j}{2}\int_0^{-u} \exp\left(-j\pi\alpha^2/2\right) d\alpha \tag{3.7}$$

where u is a scaled distance parameter. A plot of $|E/E_0|$ is given in Figure 14, and shows that at $0.6F_1$, the free space (direct path) value is obtained, where F_1 is the radius of the first Fresnel zone.

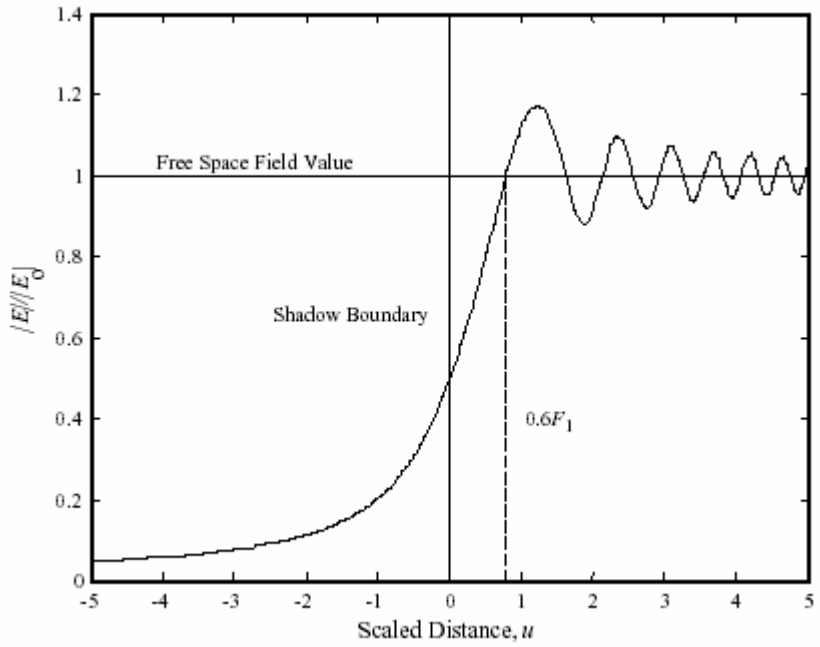

Figure 14. Plot of $|E/E_0|$ (From Ref. [10]).

A brief note on Fresnel zones is appropriate at this point. The collection of points at which reflection would produce an excess path length of $n\lambda/2$ (n an integer) is called the n^{th} Fresnel zone [10]. As seen in Figure 15, the surfaces are ellipsoids which are centered on the direct path between the transmitter and receiver.

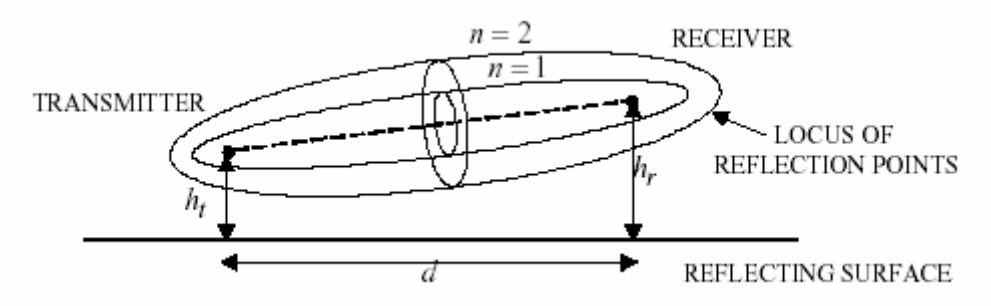

Figure 15. Fresnel zones (From Ref. [10]).

The radius of the n^{th} Fresnel zone, F_n is

$$F_n = \sqrt{\frac{n\lambda d_t d_r}{d}} \,. \tag{3.8}$$

The geometry parameters are illustrated in Figure 16.

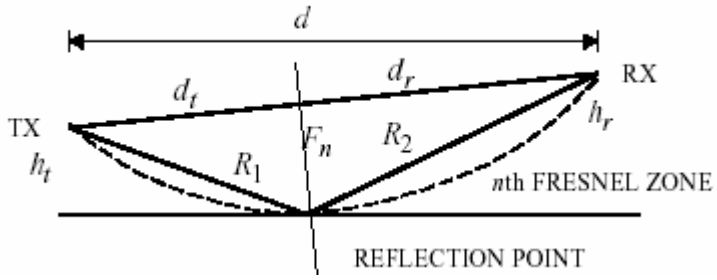

Figure 16. Radius of the n^{th} Fresnel zone (From Ref. [10]).

While designing the transmission path, it is important to put the transmitter and receiver in locations such that the reflection points do not lie on even Fresnel zones. Furthermore the LOS should clear all obstacles by $0.6F_1$ in order to achieve free space propagation levels.

3. Empirical Models for Urban Propagation

Several empirical models have been developed to overcome the limitations and assumptions presented by theoretical models. They are based on measured data and use curve-fit equations to model propagation. These models are often city-specific. For instance, Ibrahim and Parsons use London as the test environment. In the same manner,

Okumura conducted his experiments in Tokyo. However, the Okumura model can be adapted to other cities in the world by using correction factors [13].

a. The Okumura Signal Prediction Method

Okumura carried out the tests in Tokyo over a wide range of frequencies (at 200, 435, 922, 1320, 1430 and 1920 MHz), several fixed-site and mobile antenna heights (30 m to 1000 m) and over various irregular terrains and environmental clutter conditions to generate a set of curves relating field strength versus distance for a range of fixed-site heights at several frequencies [12]. Curves were then generated that extracted several behaviors in various environments. These behaviors contained the distance dependence of field strength in open and urban areas, the frequency dependence of median field strength in urban areas, and urban versus suburban differences. The limitation of this model is its dependence on curves. Since they are inconvenient to use, Hata has devised mathematical fits to the curves. [14]

b. The Hata and Modified Hata Formulas

Hata's simple formula represents Okumura's measurement in the form of

$$Loss = A + B\log(d) \tag{3.9}$$

where A and B are functions of frequency, antenna heights, and terrain type, and d is the distance. The formula for median path loss is

$$\begin{aligned} L_{ccir} &= 69.55 + 26.16\log(f) - 13.82\log(H_b) \\ &\quad + \left[44.9 - 6.55\log(H_b)\right]\log(d) + a_x(H_m) \end{aligned} \tag{3.10}$$

where f is frequency in MHz, d is distance in km, and H_b is the base station height in meters. The function $a_x(H_m)$ is the mobile height correction function. In a medium city,

$$a_x(H_m) = \left[0.7 - 1.1\log(f)\right]H_m + 1.56\log(f) - 0.8\,. \tag{3.11}$$

In a large city and at 200 MHz and below,

$$a_2(H_m) = 1.1 - 8.29\log^2[1.54H_m]. \tag{3.12}$$

At 400 MHz and above,

$$a_4(H_m) = 4.97 - 3.2\log^2[11.75H_m]. \tag{3.13}$$

As to suburban areas, the path loss is adjusted by L_{ps} ($L_{ccir} - L_{ps}$), where

$$L_{ps} = -2\log^2\left[\frac{f}{28}\right] - 5.4 \tag{3.14}$$

and in open areas, the path loss is adjusted by L_{po} ($L_{ccir} - L_{po}$), where

$$L_{po} = -4.78\log^2(f) + 18.33\log(f) - 40.94. \tag{3.15}$$

There is a modified Hata formula that is used to improve accuracy relative to the Okumura curves. The formula is

$$L_{mh} = -(L_{ccir} + S_0 - S_{ks} + B_0) \tag{3.16}$$

where S_0 is the term used for the suburban/urban correction

$$S_0 = (1 - U_r)\left[(1 - 2U_r)L_{po} + 4U_r L_{ps}\right] \tag{3.17}$$

and where U_r is the urbanization parameter and takes the following values:

0 = Open area,

0.5 = Suburban, and

1 = Urban area.

It is the term S_{ks} that departs from Hata's formula to improve the accuracy with respect to the Okumura curves for the larger distances:

$$S_{ks} = \left[27 + \frac{f}{230}\right]\log\left[\frac{17(H_b + 20)}{17(H_b + 20) + d^2}\right] + 1.3 - \frac{|f - 55|}{750} \tag{3.18}$$

where f is the frequency (100-3000 MHz), H_b is the base antenna height (30-300 m) and d is the range (1-100 km and not beyond the horizon) [13].

The term B_o in Equation (3.16) accounts for the percentage of buildings on the land in the immediate grid under consideration,

$$B_o = 25\log\left(B_1\right) - 30 \tag{3.19}$$

where B_1 is the percentage of buildings on the land ($B_1 = 15.849$ nominally).

c. Ibrahim and Parsons Method-The London Model

According to the Ibrahim and Parsons model, the propagation in an urban environment depends upon the density of buildings, the heights of buildings, and land use. The qualitative description of the urban environment is also interpreted as an inherent vagueness. The measurements were done in 500 m squares in London, England. The method can also be applied to other similar cities. Ibrahim and Parsons excess propagation loss in dB is

$$L_{ip} = -[-20\log\left(0.7H_b\right) - 8\log\left(H_m\right) + \frac{f}{40} + 26\log\left[\frac{f}{40}\right] - 86\log\left[\frac{f+100}{156}\right] \tag{3.20}$$

$$+\left[40 + 14.15\log\left[\frac{f+100}{156}\right]\right]\log\left(d1{,}000\right) + 0.265L - 0.37H + 0.087U - 5.5] .$$

The parameters for Ibrahim Parsons London Model are summarized in Table 1.

Parameter	Definition	Range of Validity
L_{ip}	Ibrahim and Parsons propagation, median, dB	-
H_b	Base antenna height, m	30-300
H_m	Mobile antenna height, m	< 3
L	Land-use factor, percentage of grid covered by buildings	3-50
H	Height difference between grid containing the fixed site and grid containing the mobile, m	-
U	Urbanization factor, percentage of buildings in grid taller than three levels; outside city center U =63.2	0-100
d	Range, km (not beyond radio horizon)	< 10
f	Frequency, MHz	150-1,000

Table 1. Parameters for the London Model.

B. URBANA WIRELESS TOOLSET

1. Introduction

Urbana is a computational electromagnetic tool for simulating wireless propagation and near-field radar sensors in complex environments [15]. The ray-tracing engine of the toolset is coupled with proprietary algorithms to implement physical optics, geometrical optics and diffraction physics in producing a three-dimensional (3-D) simulation. Antenna, network and radar system designs can be assessed for the urban environments, building interiors and automobile traffic.

Urbana provides wireless system planners with a powerful tool to simulate propagation both in outdoor rural and urban settings. It is always difficult to characterize these complex environments with simple formulas. The engineers basically have two options for system design: (1) trial-and-error and (2) propagation simulation tools. The first option is more expensive and time consuming, and not flexible for 'what if' scenarios. The simulation alternative has the advantage of flexibility and it provides the capability to analyze multiple 'what if' scenarios. It is a useful tool for the development of new systems based on new concepts.

As a summary, *Urbana* specifically can be used to [15]:

- Predict area field coverage, fading, and co-channel interference
- Conduct parametric antenna pattern and polarization studies
- Predict multiple propagation paths, distinguished by signal strength, angle of arrival, and delay
- Perform comparative studies for base station placement
- Visually establish 3-D line-of-site paths with respect to buildings, terrain, trees, etc.
- Visually identify multi-path and diffraction propagation mechanisms.

2. Principles of Operation

The *Urbana* Wireless Toolset is comprised of three programs. They are *Urbana*, *Xcell* and *Cifer*.

Urbana is the computational engine that determines the signal levels for the specified simulation inputs. The typical inputs are frequency, antenna types and building

geometry. There are several electromagnetic algorithms to choose from, but all are based on a high frequency assumption.

Xcell is used to view and modify the building and environment models that are input to *Urbana*. It can display a 3-D model and perspective views of signal strengths in and around buildings. The signal levels computed by *Urbana* can be plotted as contours. *Xcell* can also be used to remove facets or change their material assignments.

Cifer can generate simple buildings or translate building files imported from other drawing programs, or write them into the facet file format required by *Urbana.*

In addition to these three programs, there are several ancillary programs such as *f2f.x* and *bobv.x* that are used to format and translate data for post processing. The *Urbana* suite of software codes is illustrated in Figure 17. Each of the three steps shown in Figure 17 is discussed in the following sections.

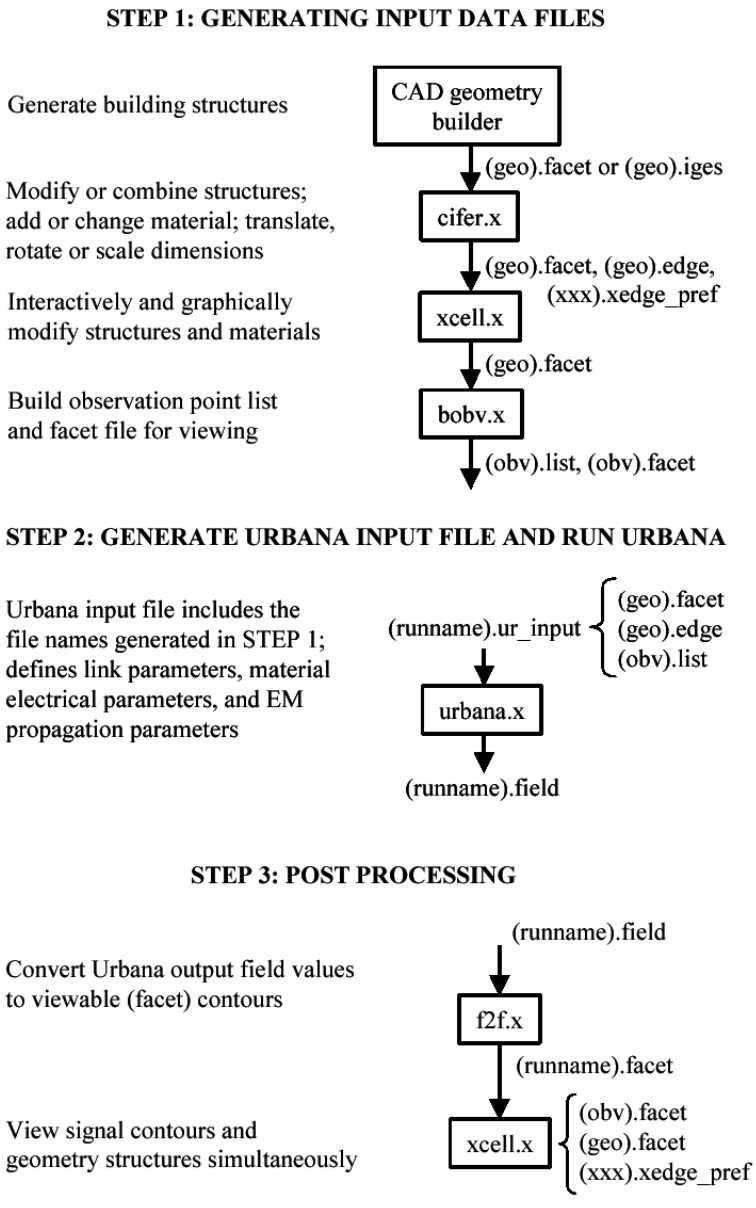

Figure 17. *Urbana* suite of software codes (From Ref. [12]).

a. Generating Input Data Files

In *Urbana*, physical objects are represented by surfaces comprised of triangular facets. These models can be generated by computer aided design (CAD) software but it is essential to convert the output file to the DEMACO facet file format. *Cifer* also can be used to generate simple objects such as curves, boxes and planes. After generating the models the material characteristics can be designated by the input variable ICOAT in the *Urbana* input file. The edges of the models have to be added to the simulation to take the diffraction calculations into consideration. *Cifer* is used for this purpose.

Building a two-dimensional array of observation points over the terrain or structure is needed for the *Urbana* program. The observation area of interest generally has the same dimensions as the ground plane. For this purpose either *bobv.x* or the *Matlab* code in Appendix B can be used. The original file of the ground plane can also be used as the name of the facet file describing the terrain. Below is a simple script for the observation points:

example_plane.facet	(indicates the name of the file)
1.0	(specifies the length unit of observation area- 1 meter)
1 1 10	(number of blocks, footprint size and dummy input variable)
1	(signifies that observation area is rectangular region)
-300.0 300.0 -200.0 200.0 2.0 4.0	(*x* and *y* region limits, delta and the offset).

After specifying the inputs, *bobv.x* (build observation points program) is executed. Upon execution, an observation list file (to be used by *Urbana*) and observation facet file (to be used by *Xcell*) are created. The difference between *bobv.x* and the *Matlab* code is that *bobv.x* can only create observation points outside of the buildings whereas *Matlab* can do it at any location [10].

b. Generating Urbana Input File and Run Urbana

The *Urbana* input file should have the extension of **.ur_input.* The text editor application, *Jot* or *Nedit*, can be used to generate it. It has the command lines to

provide the information and parameters listed below, and are modified as needed for different simulations:

- City geometry file, length and frequency units
- Antenna description and parameters
- Observation point parameters
- Theoretical considerations
- Coating materials
- Optional advanced features.

A sample input file is shown in Appendix A.

To run *Urbana* in a shell window, one should simply type "*urbana example.ur_input 1*". The parameter 1 asks for some intermediate information to be displayed (use a 0 for no display).

c. Post Processing

Two post-processing steps were used. The first was converting *Urbana* output field values to viewable (facet) contours with *f2f.x*. *Urbana* writes several output files, the most important one is the field file. The *f2f.x* program is used to convert the *Urbana* field file to viewable facet contours for *Xcell.* A generic input response to *f2f.x* is shown in Table 2.

INPUT PARAMETERS	RESPONSE
Type of E-Field	4- Magnitude of E-total
Number of Field Files	1
Name of Field File	citywgrnd2.field
Antenna Power Level	1
Histogram Interval	10 (a rough distribution of the data is displayed for scaling)
Max. and Min. Clip Values	40 dBm, -40 dBm (clipped data is removed; the background will be visible)
Max. and Min. Range Values	40 dBm (this will be red), -40 dBm (this will be blue)
Number of Levels	25 (always 25- the number of colors from blue to red)
Lowest Coating Code	1 (always 1 – code 0 is black)
Name of Output Facet File	citywgrnd2.facet (must have .facet to view in Xcell.)
Side of Footprint Square	12 (the observation cell size is 12 by 12 inches, set earlier in the execution of bobv.x)
Shift According to Z-data	Y (these determine whether the contours are plotted in the obv plane, some other flat plane, or conform to the geometry heights in the file
Enter z-offset footprint	0

Table 2. Input parameters and responses for f*2f.x*.

The second was viewing signal contours and sending them from SGIs to PCs. Xcell displays the facet file converted by f2f.x in the previous step. Since the SGI machines are in the lab environment, it is convenient to send these files to PCs to work with them. Media Recorder is a tool to achieve this goal. The images on SGI machines are in "rgb" format. The command to convert them to "jpg" is dmconvert:

dmconvert –f jfif <image1.rgb> < image1.jpg>.

After converting, the *WS-FTP* program on a network PC should be used for transferring the images from SGIs to PCs.

d. Differential Signal Plots with f2fd

After generating the field files both for the transmitter and the jammer, *f2fd* is used to take the difference between the two and to plot it in *Xcell* by converting them to facet files. The resulting contours represent S/J contours. The generic parameters that were required and sample answers to them are given in Table 3.

INPUT PARAMETERS	RESPONSE
Type of E-Field	Magnitude of E-Total (4)
Take absolute value of dB Difference	NO
Number of Field Files on (+) side	1
Name of Field File on (+) side	citywgrnd2.field
Antenna Power level Scale Factor	100
Number of Field Files on (-) side	1
Name of Field File on (-) side	Jammer900.field
Antenna Power level Scale Factor	1
Histogram Interval	10 dB
Max. and Min. Clip Values	-20, 130
Max. and Min. Range Values	-20, 130
Number of Levels	25
Lowest Coating Code	1
Name of Output Facet File	Diff2.facet
Side of Footprint Square	2
Shift According to Z-data	Y

Table 3. Input parameters and responses for *f2fd.x*.

3. Modeling for the Communication Jamming Scenario in *Urbana*

a. Modeling the City

An existing *Urbana* city model was used in this thesis. It was a replica of downtown Austin, Texas. The buildings were selected as concrete (0.3 m thick) with no windows or doors included. Along with the city, a semi-infinite ground plane was added. The ground plane was essential to figure out the ground reflections. Its dimensions were 600 m by 400 m $(-300 \le x \le 300, -200 \le y \le 200)$. The parameters for the ground plane were $\varepsilon' = 3$ and $\mu' = 1$. Finally, the building edges were also included to take the diffractions into consideration. Diffractions were caused by building and rooftop edges. The diagram for the city model with ground plane and building edges is illustrated in Figure 18. All units are in meters.

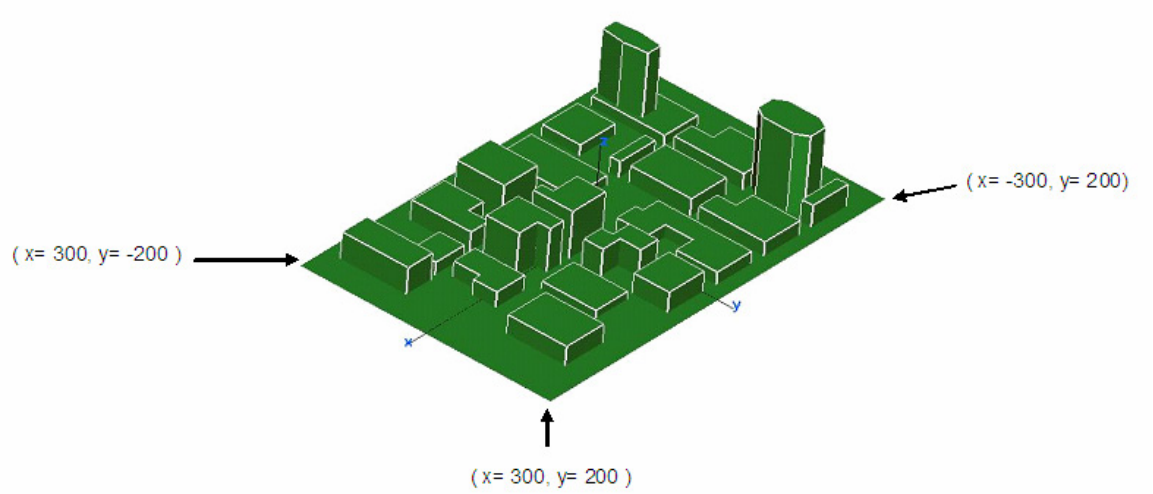

Figure 18. City model with ground plane and building edges (units in meter).

b. Modeling the Jammer and the Transmitter

The main goal of this thesis is to take jamming issues into consideration. The city was assumed to be under the enemy's control. The enemy also controlled the jammer. The antenna of the jammer was a half-wave dipole, operating at different frequencies, at the location of $(x = 0, y = -50, z = 4)$. It is illustrated in Figure 19.

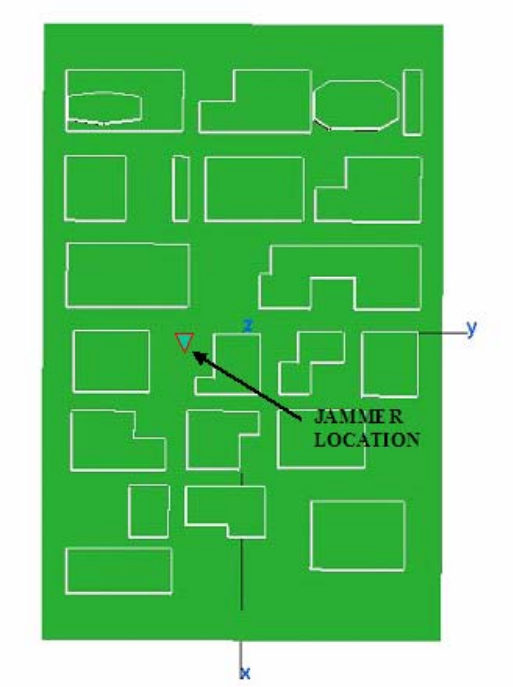

Figure 19. Jammer location (top view).

The transmitter was also a half-wave dipole. It was mounted on a UAV flying over the city at 150 m. Different locations were tried. Transmitter power was taken as 1 W. The UAV was flying from the location of (x = -250, y = 175, z = 150) to the location of $(x = -250, y = 175, z = 150)$, as seen in Figure 20. Five different locations including the starting and finishing points were simulated. The coordinates on this flight path are given in the Table 4 below.

Location	z **(m)**	x **(m)**	y **(m)**
1	150	-250	175
2	150	-200	150
3	150	-175	100
4	150	-150	0
5	150	-100	-50

Table 4. Coordinates of Locations on the flight path.

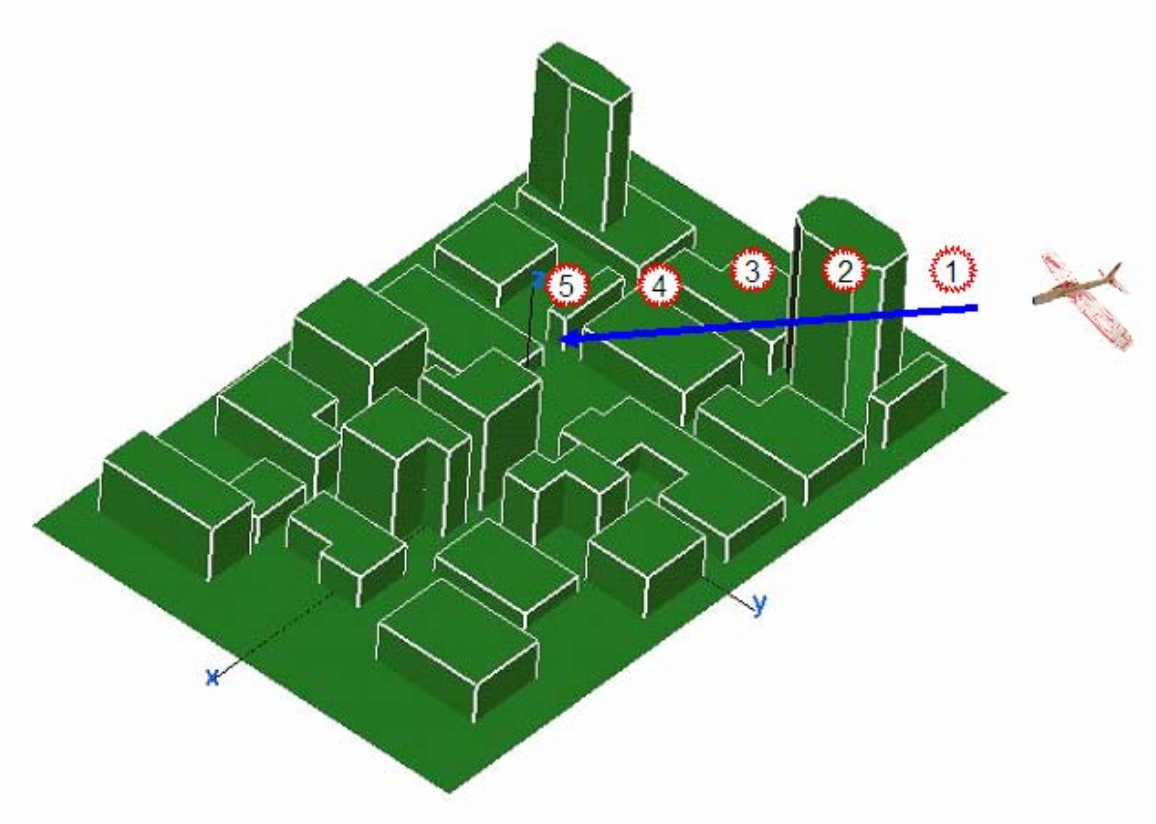

Figure 20. UAV Flight Path.

c. Generating the Observation File

Matlab software was used to generate the observation plane. The code is given in Appendix B. The observation plane has the same dimensions as the ground plane (600 m by 400 m). The name of the file used in the thesis is *obs_plane_2m.txt.* It is at a height of 2 m. Using a step size of 2, a total of 60,501 observation points were created. Choosing the number of observation points is a tradeoff. Even though many points can give a clearer picture and high resolution, it increases the running time and memory requirements.

C. SUMMARY

In this Chapter, some of the important relevant propagation mechanisms and both theoretical and empirical models for studying urban propagation were discussed. The propagation mechanisms encountered in cities were basically grouped into *reflection*, *diffraction*, *scattering* and *absorption* and they were explained briefly. Even though there have been studies explaining the urban propagation with theoretical and empirical

models, it is always difficult to characterize the complex environments such as cities with simple formulas. Engineers need propagation simulation tools to be able to design systems and to analyze multiple ‘what if’ scenarios. *Urbana* was proposed as one of these tools and it provides wireless system planners with a powerful tool to simulate propagation both in outdoor rural and urban settings.

In the next Chapter, characteristics of urban radio wave propagation and effectiveness of diversity techniques on the link performance against the jamming effects are simulated and examined.

IV. SIMULATIONS AND ANALYSIS

In this Chapter, characteristics of urban radio wave propagation and the effectiveness of diversity techniques on the link performance against jamming are simulated and examined. The diversity techniques studied here are polarization diversity and frequency diversity. The polarization diversity study includes a transmitter on a UAV and a ground based jammer. The jammer is targeting the ground based receivers used by the troops. While the transmitter is modeled to be both vertically and horizontally polarized, the jammer is always taken as vertically polarized in the simulations. As to frequency diversity techniques against a vertically polarized jammer, three different center frequencies with 50 MHz bandwidth are considered. The center frequencies are 0.9 GHz, 2.4 GHz and 5 GHz. In the last section of the simulations, a vertically polarized transmitter at 0.9 GHz with different power levels is studied. The goal is to see the effects of power increase in overcoming the jammer.

A. SIMULATIONS OF DIFFERENT POLARIZATIONS VS JAMMING

1. Simulations with Vertically and Horizontally Polarized Transmitter

a. Vertically Polarized Transmitter

First of all, the power radiated from the transmitter antenna, which was a half-wave dipole mounted on the UAV, was found. As mentioned in Chapter III, the UAV was flying over the city at 150 m. Simulations were done for five different locations and the power levels were found on the observation plane at the height of 2 m. The antenna frequency was 0.875 GHz, and the transmitting power was 1 W. Simulations started with calculating the power levels for vertical polarization. The results are summarized in Table 5. The values of the maximum and minimum power levels over all observation points are listed. The lowest threshold is -200 dBm. The lower minimum values indicate deeper shadows. It should be pointed out that it is the number of points below the minimum signal power to maintain the link that is of interest, as will be discussed later.

Location	Coordinates (m)	Power Min (dBm)	Power Max (dBm)
(1)	(-250, 175, 150)	-200.00	-2.14
(2)	(-200, 150, 150)	-91.17	-1.04
(3)	(-175, 100, 150)	-67.31	-0.65
(4)	(-150, 0, 150)	-73.00	0.05
(5)	(-100, -50, 150)	-62.82	-1.54

Table 5. Power levels for Vertical Polarization at 0.875 GHz.

Figures 21 through 25 show the plots for the five UAV locations in Table 5. A red star shows the location of the UAV on the flight path. The dynamic range, which is basically the difference between range maximum and range minimum for the color bar on the right hand side of the plots, is 70 dB.

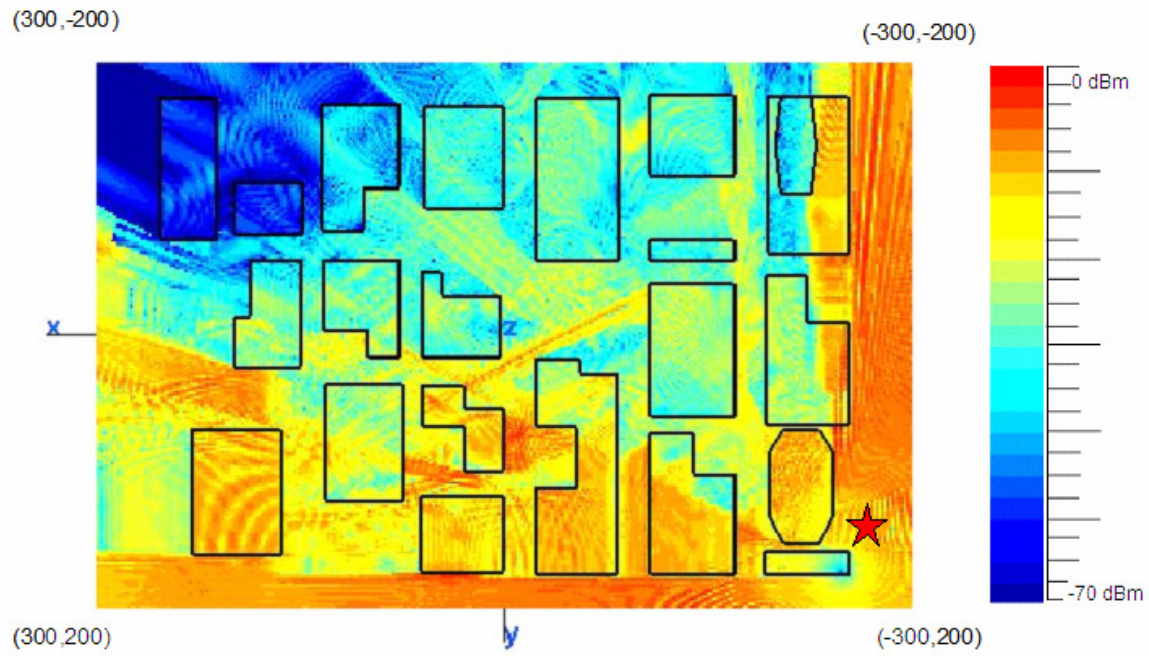

Figure 21. Transmitter at Location 1 (-250, 175, 150).

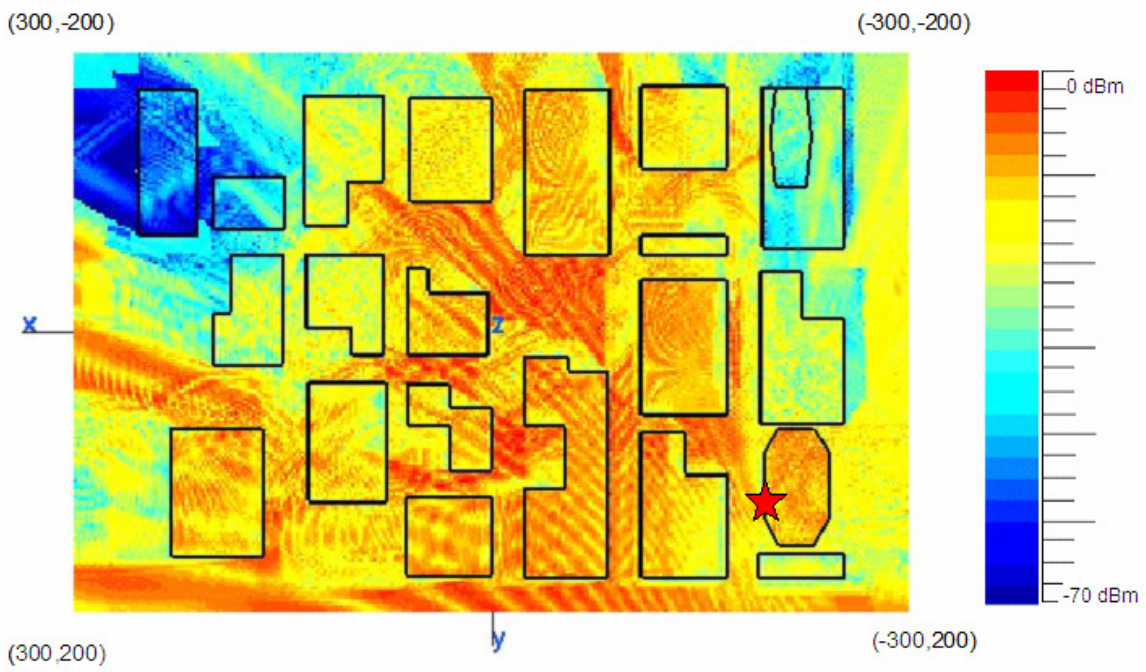

Figure 22. Transmitter at Location 2 (-200, 150, 150).

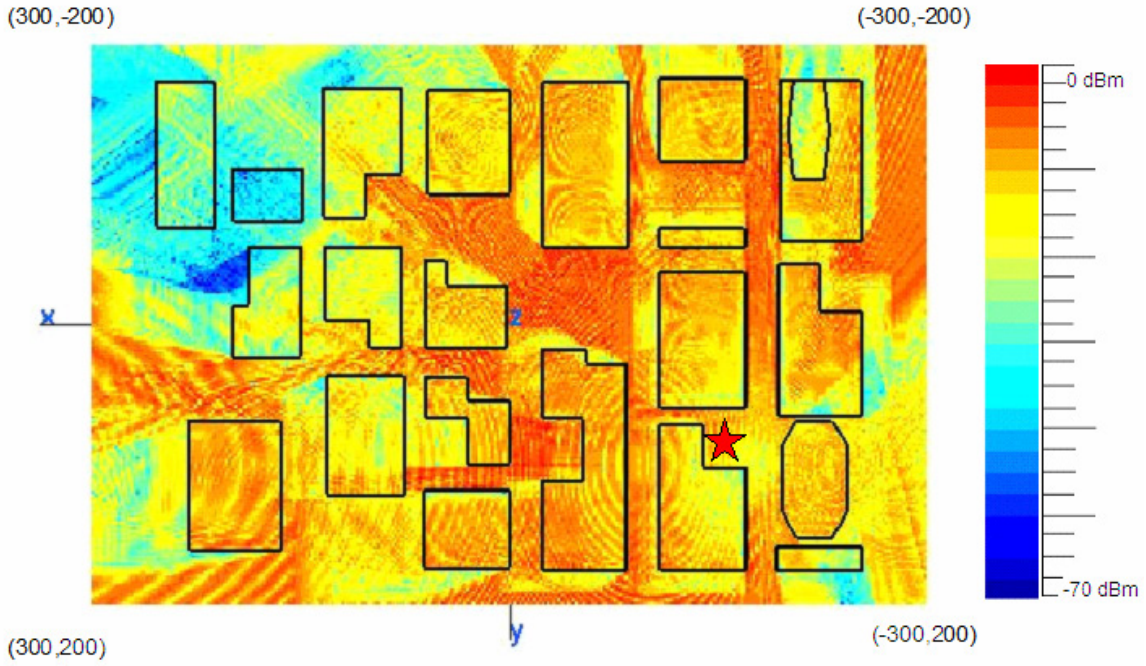

Figure 23. Transmitter at Location 3 (-175, 100, 150).

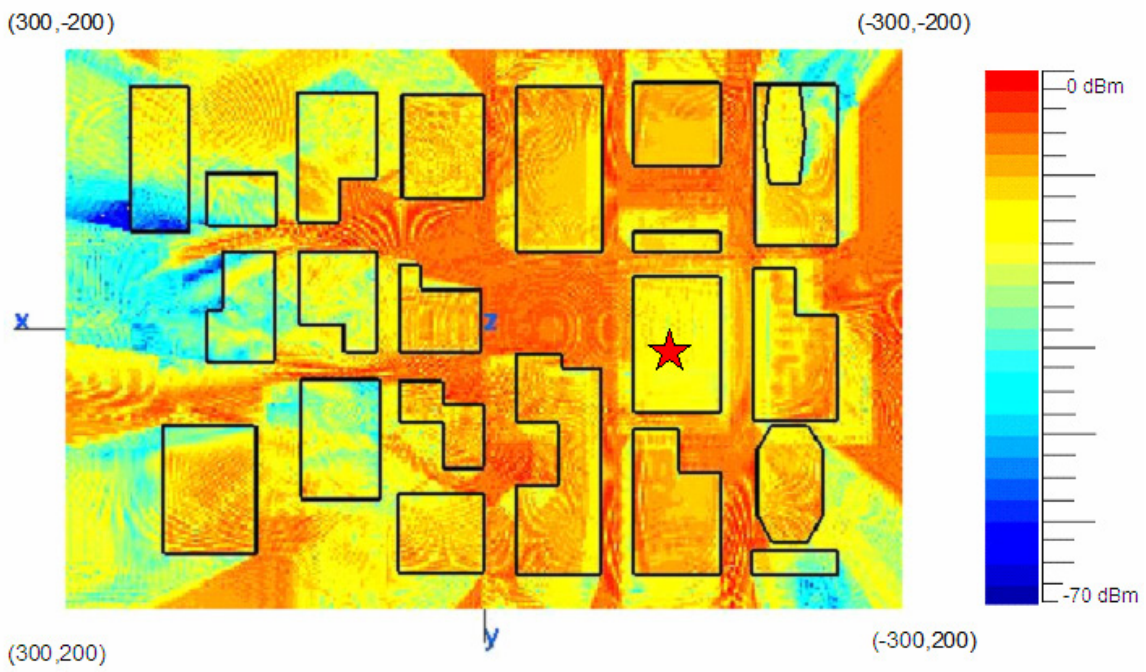

Figure 24. Transmitter at Location 4 (-150, 0, 150).

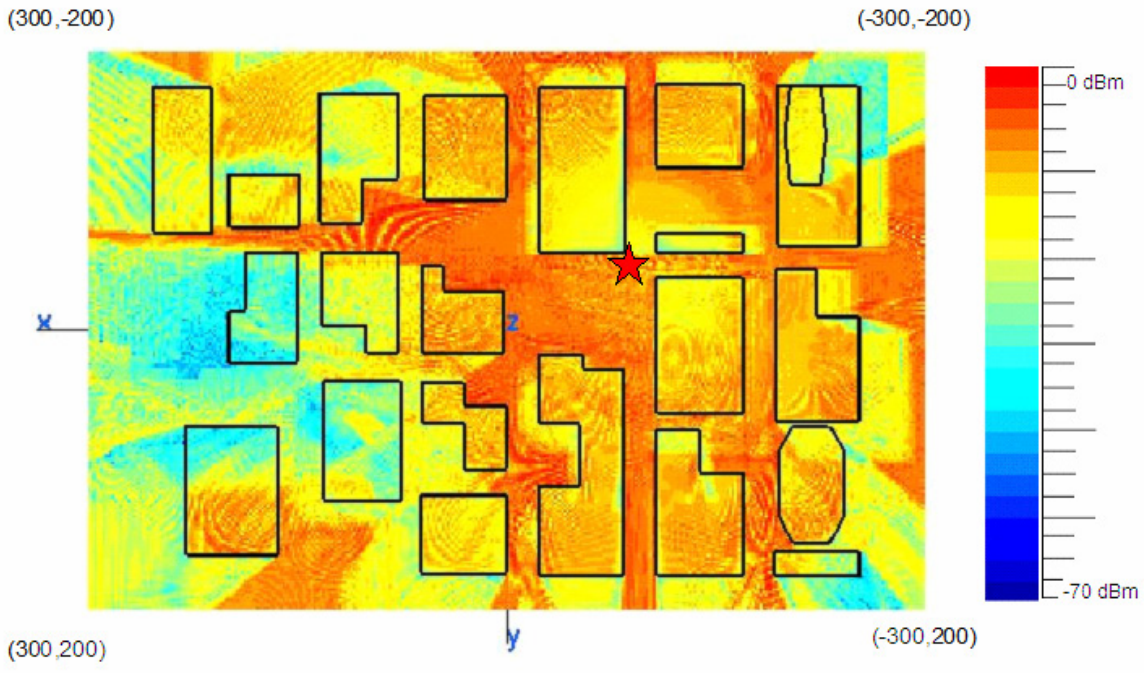

Figure 25. Transmitter at Location 5 (-100, -50, 150).

b. Horizontally Polarized Transmitter

Now, the polarization of the antenna is changed from vertical to horizontal. To make this change, the *Urbana* input file was modified as follows: "B3: Create Antenna List, Line2: Local x-axis in main coordinate" was changed from (1. 0. 0.) to (0. 0. -1) and "Line2: Local z-axis in main coordinate" was changed from (0. 0. 1.) to (1. 0. 0.). This means the antenna rotation vectors are changed to $\hat{x}_{ant} = -\hat{z}$ and $\hat{z}_{ant} = \hat{x}$ relative to the main coordinate system. The flight path, frequency, power and the observation plane were the same in order to see the polarization effect. Table 6 summarizes the results.

Location	Coordinates (m)	Power Min (dBm)	Power Max (dBm)
(1)	(-250, 175, 150)	-200.00	6.05
(2)	(-200, 150, 150)	-200.00	5.01
(3)	(-175, 100, 150)	-72.97	4.88
(4)	(-150, 0, 150)	-80.63	4.69
(5)	(-100, -50, 150)	-66.86	3.02

Table 6. Power levels for Horizontal Polarization at 0.875 GHz.

Figures 26 through 30 show the plots for the five locations. A red star shows the location of the UAV on the flight path. The dynamic range is 70 dB.

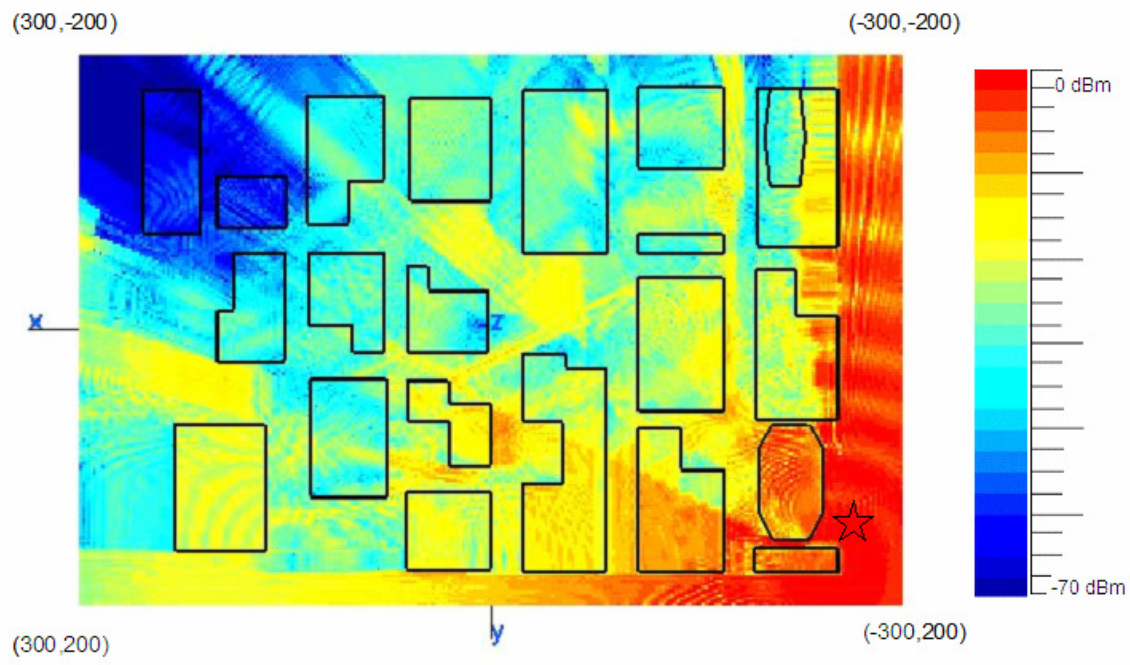

Figure 26. Transmitter at Location 1 (-250, 175, 150).

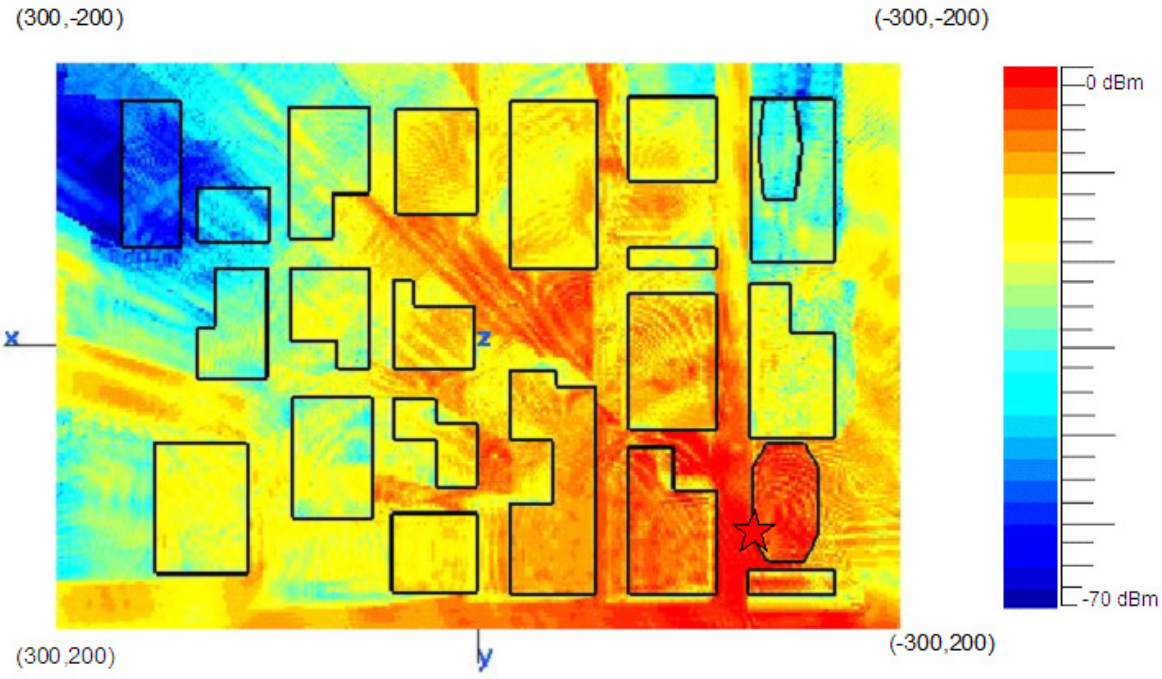

Figure 27. Transmitter at Location 2 (-200, 150, 150).

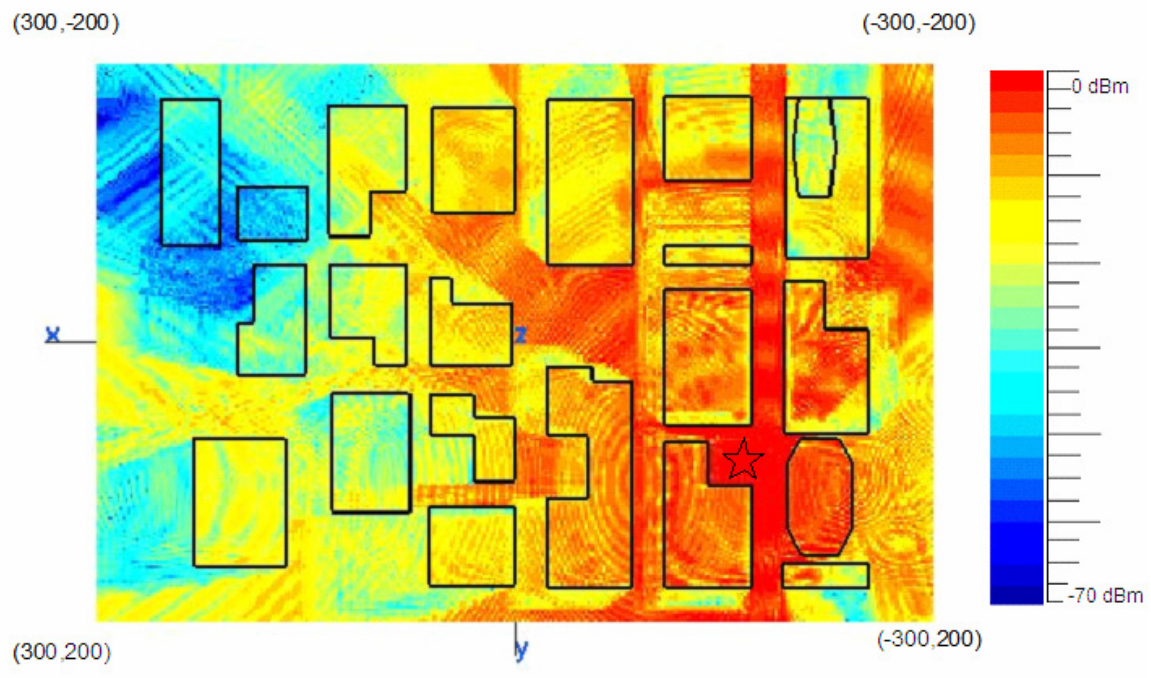

Figure 28. Transmitter at Location 3 (-175, 100, 150).

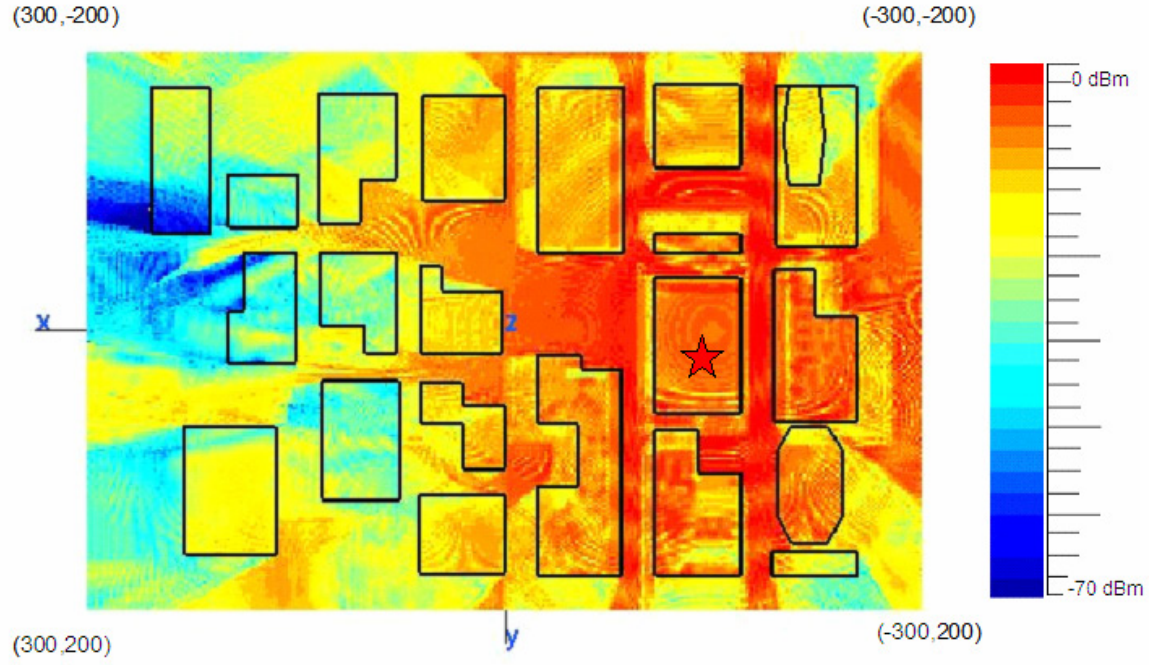

Figure 29. Transmitter at Location 4 (-150, 0, 150).

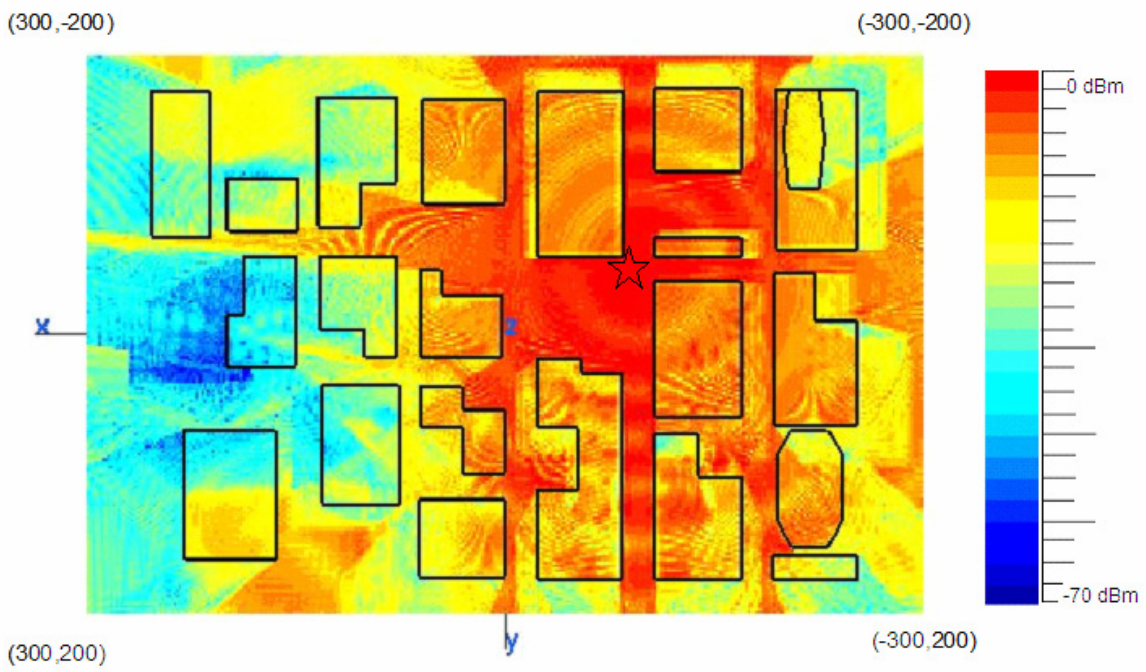

Figure 30. Transmitter at Location 5 (-100, -50, 150).

For comparison it is better to see the results for vertical and horizontal polarizations in the same table. Table 7 lists the power levels for both polarizations.

Location	Polarization vs. Power Min (dBm)		Polarization vs. Power Max (dBm)	
	Vertical	Horizontal	Vertical	Horizontal
1	-200.00	-200.00	-2.14	6.05
2	-91.17	-200.00	-1.04	5.01
3	-67.31	-72.97	-0.65	4.88
4	-73.00	-80.63	0.05	4.69
5	-62.82	-66.86	-1.54	3.02

Table 7. Comparison of Power Levels for Vertical and Horizontal Polarizations.

From Table 7 it might be interpreted that signal levels are better for the vertically polarized transmitter in terms of the minimum power, whereas the horizontally polarized transmitter provides higher signal levels in maximum power. However, we can not conclude much based on maximum and minimum values. When Figures 21 through 30 are examined, overall we may conclude that the vertically polarized transmitter gives

better results compared to the horizontally polarized antenna since the signals shown in red cover a wider area in the vertically polarized case. A potential problem for vertical polarization is that the antenna null is pointed down. Therefore a receiver under the antenna sees a low gain. Horizontal polarization can also be preferred when less sensitive systems, which have higher thresholds, are used by ground units.

2. Simulations with Vertically and Horizontally Polarized Transmitter against Vertically Polarized Jammer

a. Vertically Polarized Jammer

In order to see the effects of polarization diversity for the transmitter, jammer characteristics such as antenna type, frequency, location, transmitting power and polarization were assumed to stay fixed. The antenna of the jammer was a half-wave dipole, operating at a frequency of 0.9 GHz at the location of $(x=0, y=-50, z=4)$. The antenna power was chosen as 1 W. The jammer antenna polarization type was vertical polarization. Figure 31 shows the jammer power distribution plot generated by the simulation. The inverse triangle denotes the jammer location.

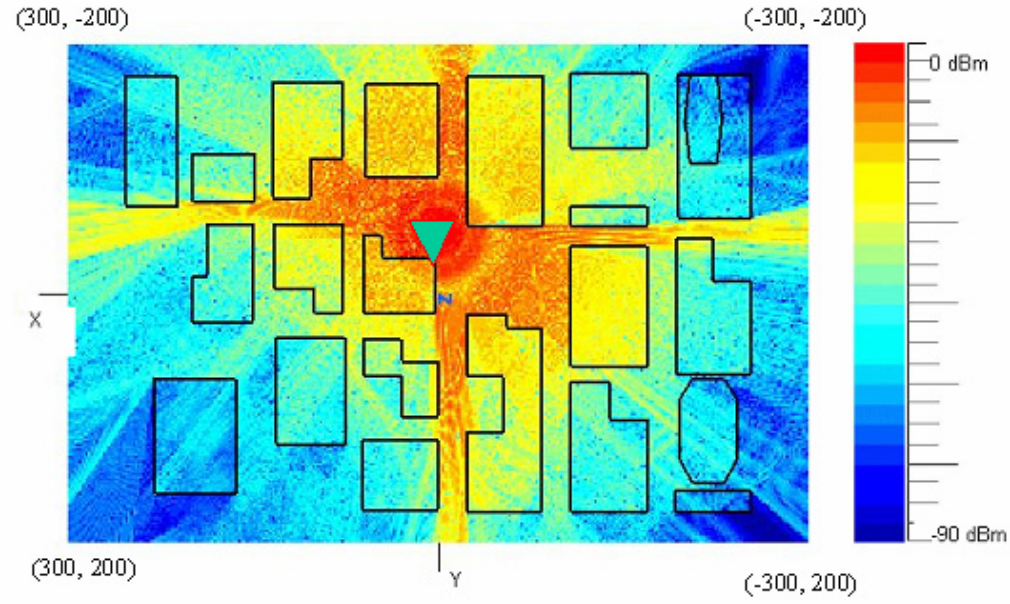

Figure 31. Vertically Polarized Jammer at 0.9 GHz.

b. Vertically Polarized Transmitter Effectiveness against Vertically Polarized Jammer

In this section, the effects of polarization diversity against a jammer were studied. After generating the plots for both transmitter and jammer, *f2fd* is used to find the difference between the two plots. This was the procedure used for all simulations to determine the effectiveness of the transmitter when being jammed. The signal-to-jam Ratio (S / J) is expressed in dB, which is accomplished by putting the transmitter file on the (+) side and the jammer file on the (-) side in the *f2fd* input. This is equivalent to a noncoherent jammer; the ratio of powers is used in computing the SJR. For this study, the values of SJR greater than 0 dB were assumed to be enough for the communication links in the city. This is called the jammer burnthrough condition. Table 8 illustrates the results for vertically polarized transmitter antenna operating at 0.875 GHz and transmitting 1 W against the vertically polarized jammer operating at 0.875 GHz also transmitting 1 W.

Location	Name of Field File on (+) side (Transmitter)	Name of Field File on (-) side (Jammer)	$(S/J)_{min}$ (dB)	$(S/J)_{max}$ (dB)
1	Citywgrnd5.field	Jammer875.field	-149.41	191.68
2	Citywgrnd2.field	Jammer875.field	-36.72	169.79
3	citywgrnd3.field	Jammer875.field	-33.64	181.98
4	Citywgrnd1.field	Jammer875.field	-28.48	165.46
5	Citywgrnd4.field	Jammer875.field	-27.77	173.16

Table 8. Transmitter Effectiveness for Vertically Polarized Antenna.

Figures 32 and 33 show the difference in plots for UAV Location 1 (the farthest point from the jammer) and for Location 5 (the closest point to the jammer). Locations with blue color are below 0 dB and communications in those places are disrupted by the jammer. Locations with red color are the places that the transmitter can overcome the jammer and the communication link can be established between the UAV relay and the receivers carried by ground units. The star represents the transmitter and the inverse triangle represents the jammer. The dynamic range is 400 dB.

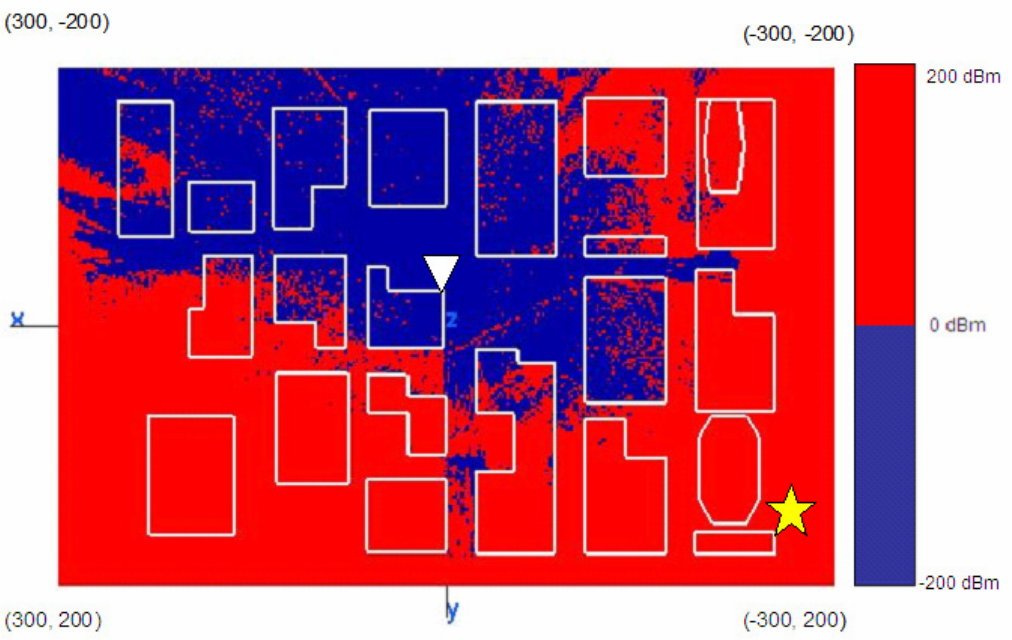

Figure 32. Vertically Polarized Signal-to-Jam Ratio with the Transmitter at Location 1.

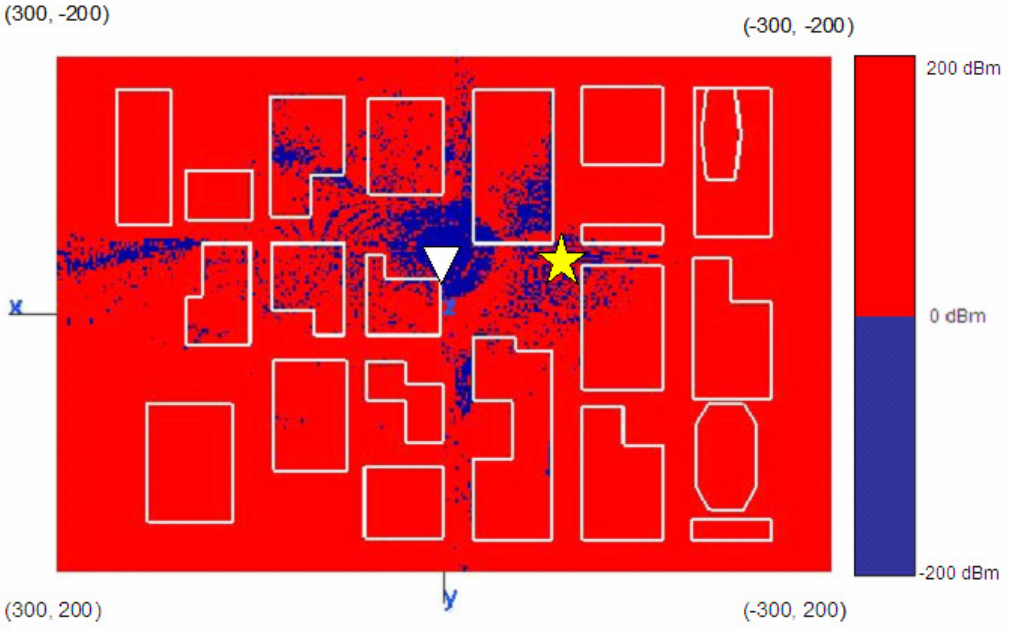

Figure 33. Vertically Polarized Signal-to-Jam Ratio with the Transmitter at Location 5.

Table 8 and Figures 32 and 33 show that the jammer is less effective when the transmitter is close to the jammer. The reason for this is due to the fact that the

jammer signal is blocked by the large buildings in the city center. The UAV is operating at a high altitude, so its signal is not blocked by the high buildings. The minimum power difference is -148.53 dB in Location 1 and -28 dB in Location 5. As to the maximum power difference, it varies for each location. The apparent trend is seen in the results. When the UAV arrives at the closest point to the jammer, it can cover a wider range and overcome the jammer more effectively. Note that the conclusion would not hold if the jammer were to concentrate on the UAV receiver rather than the ground receivers.

c. Horizontally Polarized Transmitter Effectiveness against Vertically Polarized Jammer

The same operations were also done for horizontal polarization for the antenna mounted on UAV. Table 9 illustrates the results for a horizontally polarized transmitter antenna operating at 0.875 GHz and transmitting 1 W against the vertically polarized jammer operating at 0.875 GHz also transmitting 1 W.

Location	Name of Field File on (+) side (Transmitter)	Name of Field File on (-) side (Jammer)	$(S/J)_{min}$ (dB)	$(S/J)_{max}$ (dB)
1	citywgrnd10.field	Jammer875.field	-149.41	194.34
2	Citywgrnd7.field	Jammer875.field	-125.90	178.59
3	Citywgrnd8.field	Jammer875.field	-42.11	182.02
4	Citywgrnd6.field	Jammer875.field	-42.87	171.34
5	Citywgrnd9.field	Jammer875.field	-23.13	172.49

Table 9. Transmitter Effectiveness for Horizontally Polarized Antenna.

Figures 34 and 35 show the difference in plots for Location 1 (the farthest point from the jammer) and for Location 5 (the closest point to the jammer). The star represents the transmitter and inverse triangle represents the jammer. The dynamic range is 400 dB. Like the vertically polarized case, the horizontally polarized transmitter has better coverage when it is over Location 5.

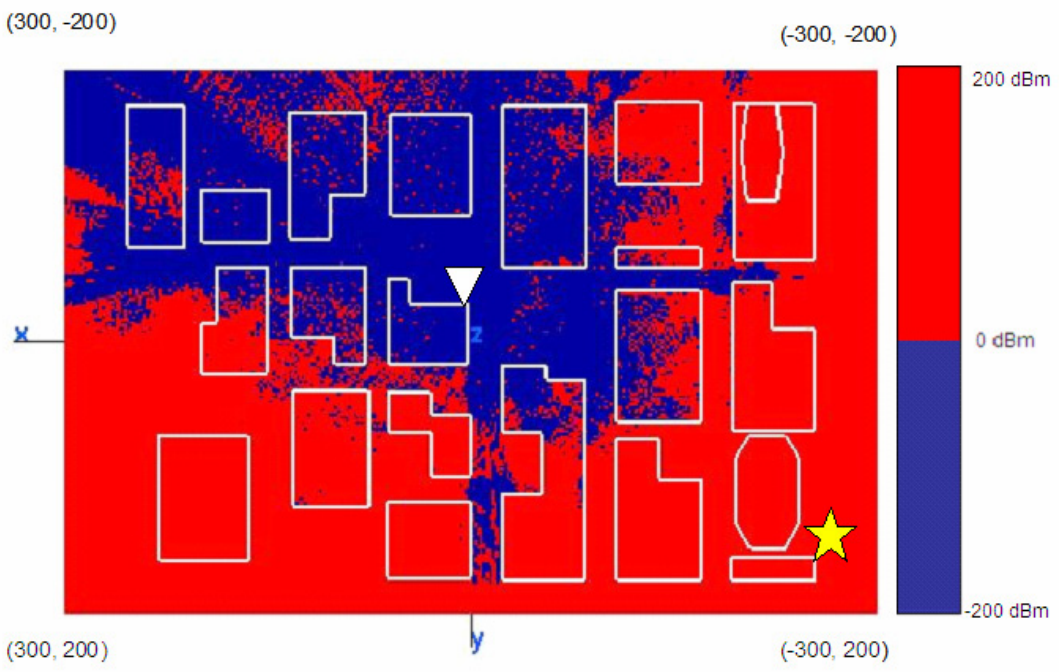

Figure 34. Horizontally Polarized Signal-to-Jam Ratio with the Transmitter at Location 1.

Figure 35.

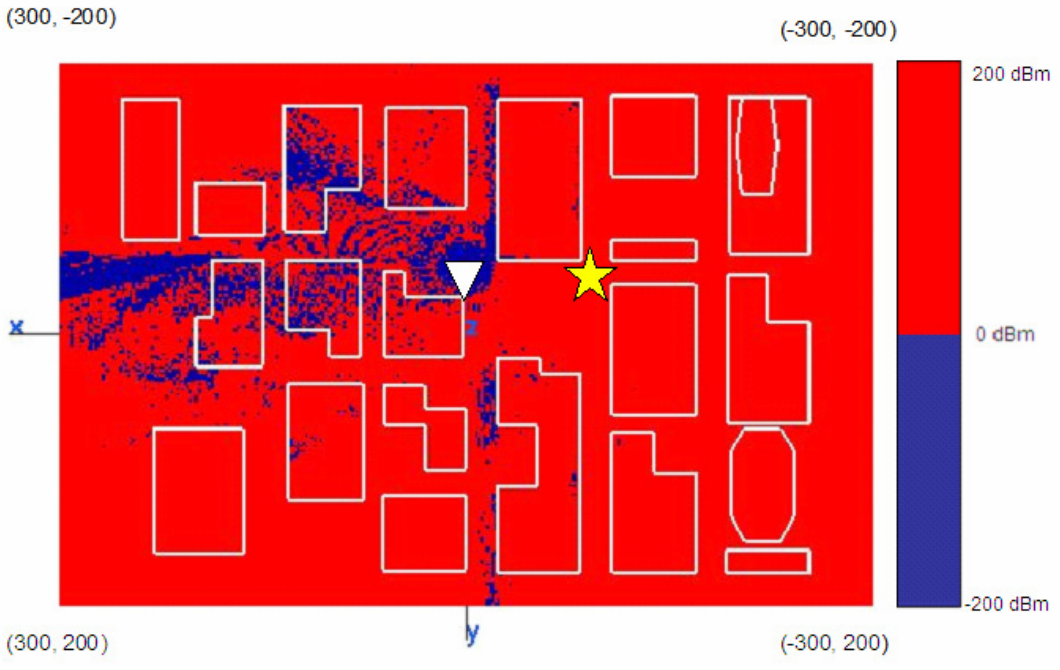

Figure 36. Horizontally Polarized Signal-to-Jam Ratio with the Transmitter at Location 5.

3. Conclusions

It is easier to see the difference between vertical and horizontal polarizations when listed side by side. Table 10 compares the power difference levels for both polarization types.

Location	$(S/J)_{min}$ (dB)		$(S/J)_{max}$ (dB)	
	Vertical	Horizontal	Vertical	Horizontal
1	-148.53	-148.53	191.68	194.34
2	-37.66	-129.86	169.00	178.59
3	-32.50	-41.15	181.98	182.02
4	-29.63	-37.54	165.46	171.34
5	-28.00	-23.01	173.16	172.49

Table 10. Comparison of Power Difference Levels for Vertical and Horizontal Polarizations.

Based on the maximum and minimum S/J, the results given in Table 10 could be deceiving. Vertical polarization seems better based on minimum power difference and horizontal polarization seems better in maximum power difference. A comparison of Figures 32 through 35 for both polarization types does not indicate a dramatic difference between them.

A better way to interpret the figures is to find the percentage of the locations blocked by the jammer (blue-colored areas) versus the percentage of the locations where communication link can be established (red-colored areas). In the observation plane, there are 60,501 points representing the possible receiver locations. In *f2fd, Urbana* gives the number of points at different signal levels. We can calculate the percentage of blue-colored and red-colored areas and determine the effectiveness (or availability) of the communication link for either polarization type. The points below 0 dB (the burnthrough condition) are assumed to be the areas where no link can be established or maintained. The points above that are red are to be the ones capable of supporting a link. Table 11 illustrates the results.

UAV Location	Polarization Type	Number of Points with S/J				Percentage (%) of Links Established	Percentage (%) of Links Jammed
		-200 to -100 dB	-100 to 0 dB	0 to 100 dB	100 to 200 dB		
1	Vertical	780	20576	39104	41	64.7	35.3
	Horizontal	780	21055	38515	151	63.9	36.1
2	Vertical	-	8326	52121	54	86.2	13.8
	Horizontal	2	9632	50752	115	84.0	16.0
3	Vertical	-	5938	54514	49	90.0	10.0
	Horizontal	-	7190	53254	57	88.1	11.9
4	Vertical	-	4295	56172	34	92.9	7.1
	Horizontal	-	5944	54521	36	90.1	9.9
5	Vertical	-	3601	56866	34	94.0	6.0
	Horizontal	-	4144	56321	36	93.1	6.9

Table 11. Percentages of Links Established and Jammed for Different Polarizations.

From Table 11, the vertically polarized transmitter has obviously higher percentages of links established for every location taken on the flight path. The highest percentage (94%) occurs at Location 5.

B. SIMULATIONS FOR DIFFERENT FREQUENCIES

In this section, the effect of frequency diversity is studied. Frequency diversity involves sending the same information independently over several frequencies in a specific bandwidth [12]. This would prevent fading due to the multipath between the transmitter and receiver. Since multipath is frequency dependent, selecting multiple frequencies that are decorelated ensures that at least one frequency is free of severe fading effects.

1. Simulations at Different Frequencies

The center frequencies are chosen in the ISM bands as 0.9 GHz, 2.4 GHz, and 5.0 GHz. The bandwidth is 50 MHz. The transmitter antenna is assumed to be vertically polarized and the UAV on which it is mounted is at Location 5. It is the closest point to

the jammer. Power for transmitter antenna is 1 W. The coordinates for Location 5 are $(x = -100, y = -50, z = 150)$. Since the antenna is approximately a half wave dipole, the dipole length varies at each frequency band. The results are given in Table 12 below.

Transmitter Center Frequency (GHz)	Transmitter Simulation Frequency (GHz)	Received Power (dBm)	
		Min	Max
0.9	0.8750	-62.82	-1.54
	0.8875	-60.76	-1.22
	0.9000	-60.64	-1.09
	0.9125	-58.87	-1.76
	0.9250	-61.35	-1.66
2.4	2.3750	-96.21	-2.32
	2.3875	-98.02	-2.51
	2.4000	-99.54	-1.86
	2.4125	-98.04	-2.75
	2.4250	-97.96	-1.36
5.0	4.9750	-152.78	-2.20
	4.9875	-153.94	-1.51
	5.0000	-151.75	-2.49
	5.0125	-150.04	-2.94
	5.0250	-151.00	-2.22

Table 12. Signal power levels at different frequencies.

Both minimum and maximum power decreases when the frequency increases. It is due to path loss, which increases when frequency increases [16]. The minimum powers are -60.94 dBm, -99.54 dBm and -151.75 dBm for 0.9 GHz, 2.4 GHz, and 5 GHz respectively. Figures 36 through 38 illustrate the signal power levels for the center frequencies. A star represents the location of the transmitter mounted on the UAV.

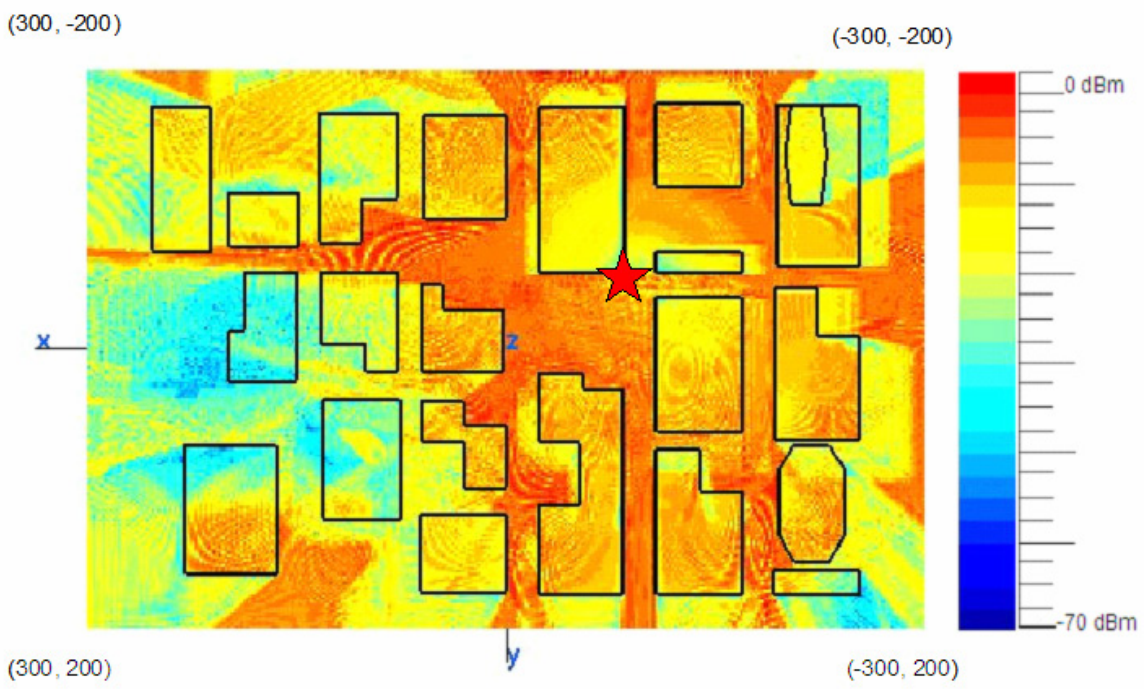

Figure 37. Vertically Polarized Transmitter at 0.9 GHz.

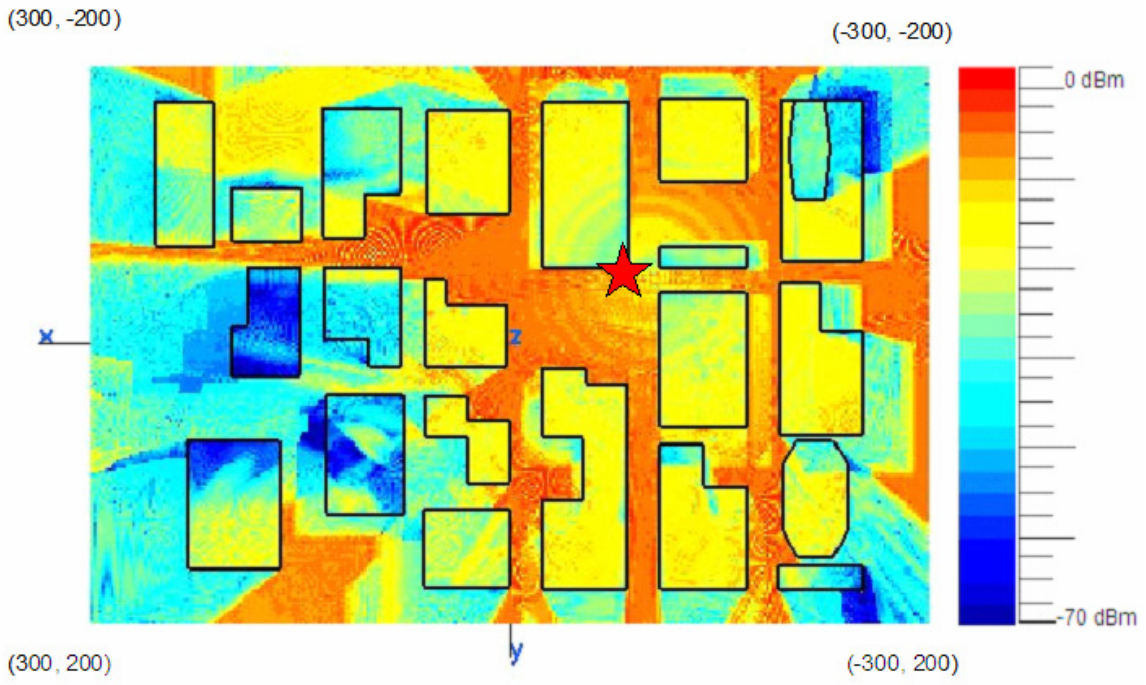

Figure 38. Vertically Polarized Transmitter at 2.4 GHz.

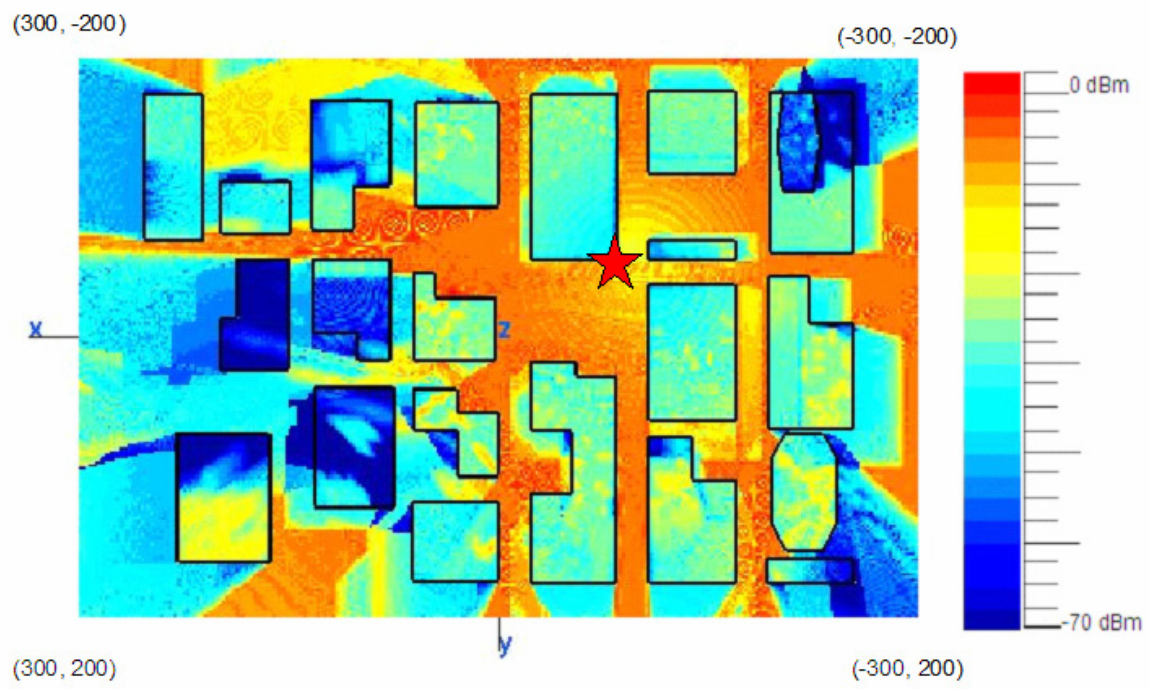

Figure 39. Vertically Polarized Transmitter at 5 GHz.

The signal level at the outer edge of the observation plane is getting smaller when the frequency increases. One reason is that the space loss increases with frequency. Also, propagation through buildings reduces dramatically at high frequencies due to the increased loss in building materials. Shadow regions generally have lower signal levels than the direct path regions. These regions are determined by changes in building arrangement and height, and the widths of streets. It is still possible to get good signal levels, even in the shadow regions, since electromagnetic waves reflect from surfaces and diffract from edges.

2. Simulations with a Vertically Polarized Transmitter and Vertically Polarized Jammer versus Frequency

The results are given in Table 13 for simulations with a vertically polarized transmitter against a vertically polarized jammer versus frequency.

Transmitter Frequency (GHz)	Jammer Frequency (GHz)	S/J (dB)	
		Min	Max
0.875	0.875	-27.77	173.16
0.900	0.900	24.22	169.15
0.925	0.925	-21.26	171.06
2.375	2.375	-32.47	149.04
2.400	2.400	-31.97	147.93
2.425	2.425	-33.41	146.73
4.975	4.975	-72.24	159.48
5.000	5.000	-72.68	164.00
5.025	5.025	-68.49	154.08

Table 13. Vertically Polarized Transmitter against Vertically Polarized Jammer at Different Frequencies.

Figures 39 through 41 show the difference in plots for the simulations with a vertically polarized transmitter against a vertically polarized jammer at different center frequencies. Only the plots for center frequencies are shown. A star represents the transmitter and an inverse triangle represents the jammer. The dynamic range is 400 dB.

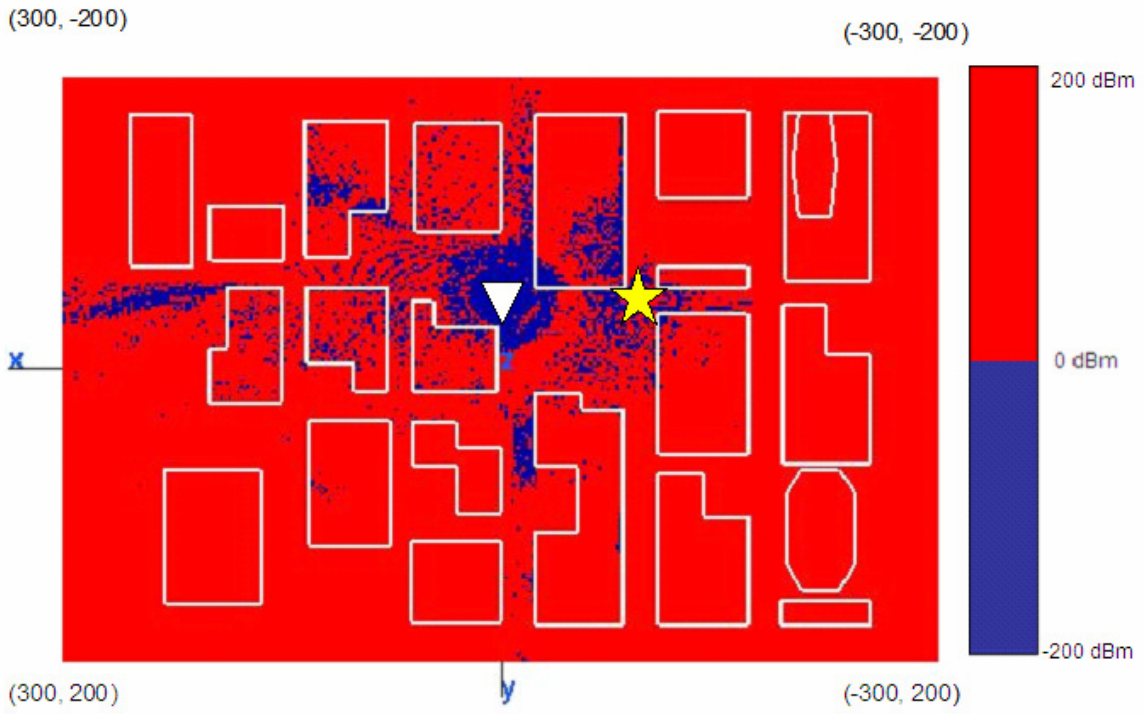

Figure 40. Signal-to-Jam Ratio for a Vertically Polarized Transmitter against Vertically Polarized Jammer at 0.9 GHz.

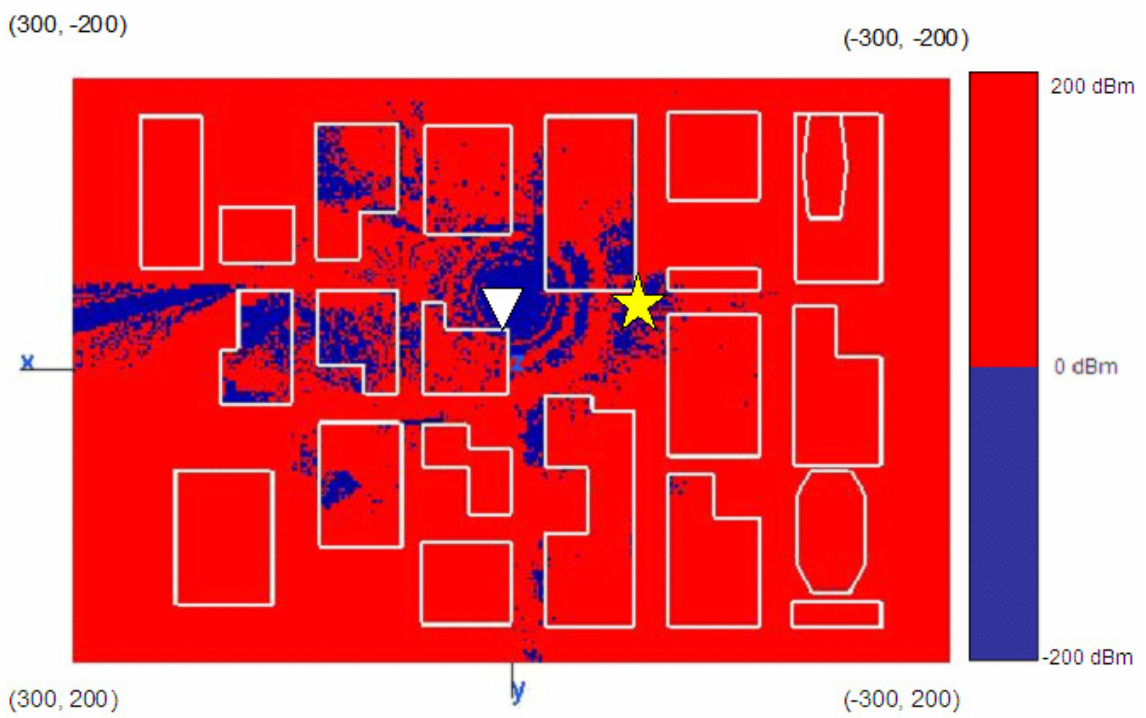

Figure 41. Signal-to-Jam Ratio for a Vertically Polarized Transmitter against Vertically Polarized Jammer at 2.4 GHz.

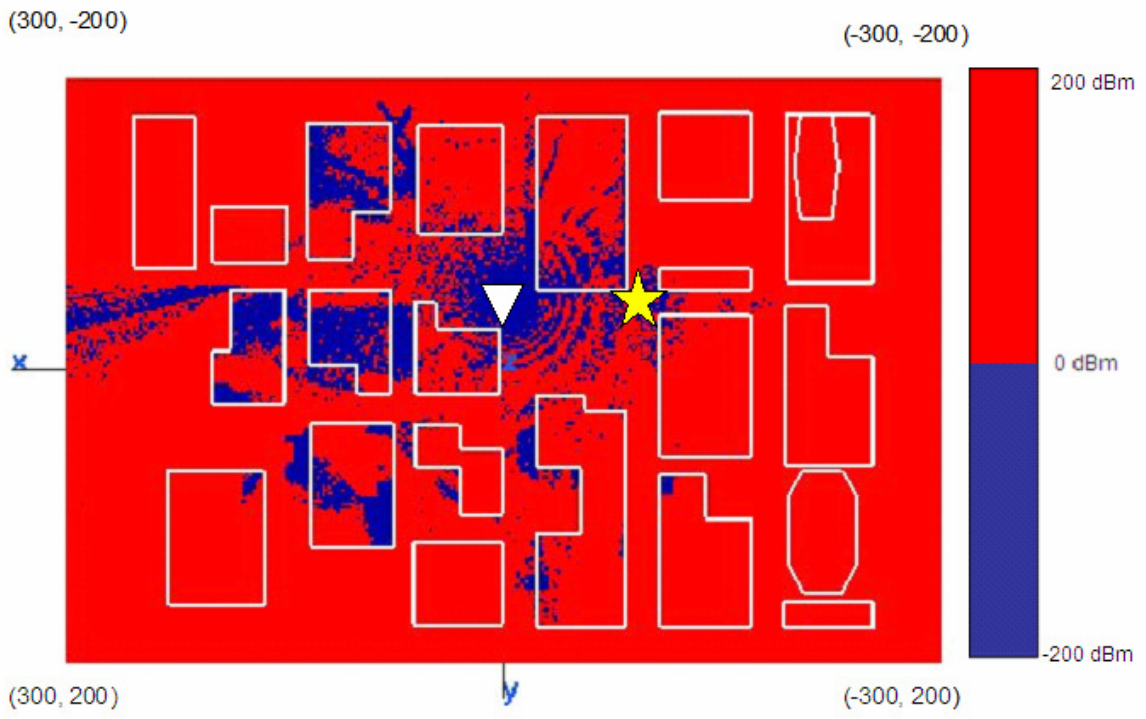

Figure 42. Signal-to-Jam Ratio for a Vertically Polarized Transmitter against Vertically Polarized Jammer at 5 GHz.

The simulations with a jammer give similar trends as the simulations without a jammer. Blue regions are getting larger when the frequency increases. Those are the receiver locations which are below S/J= 0 dB and are not getting enough signal level to communicate with the UAV. Again, the calculation of percentages of the links established and jammed gives the best insight to interpret the results. The results are given in Table 14. The percentage of good links is at the highest level of 93.7% when the center frequency is 0.9 GHz. It reduces to 91.6% at 2.4 GHz, and it reaches a low of 89.7% at the center frequency of 5 GHz.

Transmitter and Jammer Frequency (GHz)	Number of Points			Percentage (%) of Links Established	Percentage (%) of Links Jammed
	-100 to 0 dB	0 to 100 dB	100 to 200 dB		
0.875	3689	56778	34	94.0	6
0.900	3794	56673	34	93.7	6.3
0.925	4011	56456	34	93.4	6.6
2.375	5190	55265	46	91.5	8.5
2.400	5059	55394	48	91.6	8.4
2.425	4942	55514	45	91.9	8.1
4.975	6328	53266	907	89.6	10.4
5.000	6280	53278	943	89.7	10.3
5.025	6353	53182	966	89.5	10.5

Table 14. Percentages of Links Established and Jammed for Different Frequencies.

3. Conclusions

Communications at 0.9 GHz, 2.4 GHz, and 5 GHz between ground units in a city and a UAV relay flying over the city with a jammer operating in the city were simulated for 50 MHz bandwidth. Lower frequencies have better performance compared to higher frequencies. High frequencies are more attenuated in lossy materials like concrete, which is used for the building material in this study. However, higher frequencies may be

preferred since they have an advantage of higher data rates compared to lower frequency bands. There is a tradeoff in this regard.

C. SIMULATIONS WITH A VERTICALLY POLARIZED TRANSMITTER WITH DIFFERENT POWER LEVELS AGAINST A VERTICALLY POLARIZED JAMMER

In this last section of simulations, a vertically polarized transmitter at 0.9 GHz with different power levels is studied. The jammer frequency is also 0.9 GHz, and its power is 1 W. The goal is to see the effects of transmitter power increase in overcoming a jammer. The UAV is assumed to be at Location 5 (the closest point from the jammer). The results in terms of signal differences are given in the Table 15.

Location	Power Level (W)	Min. Power Difference (dB)	Max. Power Difference (dB)
5 (-100, -50, 150)	1	-24.22	169.15
5 (-100, -50, 150)	5	-17.23	176.14
5 (-100, -50, 150)	10	-14.22	179.15
5 (-100, -50, 150)	15	-12.45	180.91
5 (-100, -50, 150)	25	-10.24	183.13

Table 15. Power Differences at Different Transmitter Power Levels.

Figures 42 through 46 show the difference in plots for the simulations with a vertically polarized transmitter against a vertically polarized jammer with different transmitter power levels. The dynamic range is 400 dB.

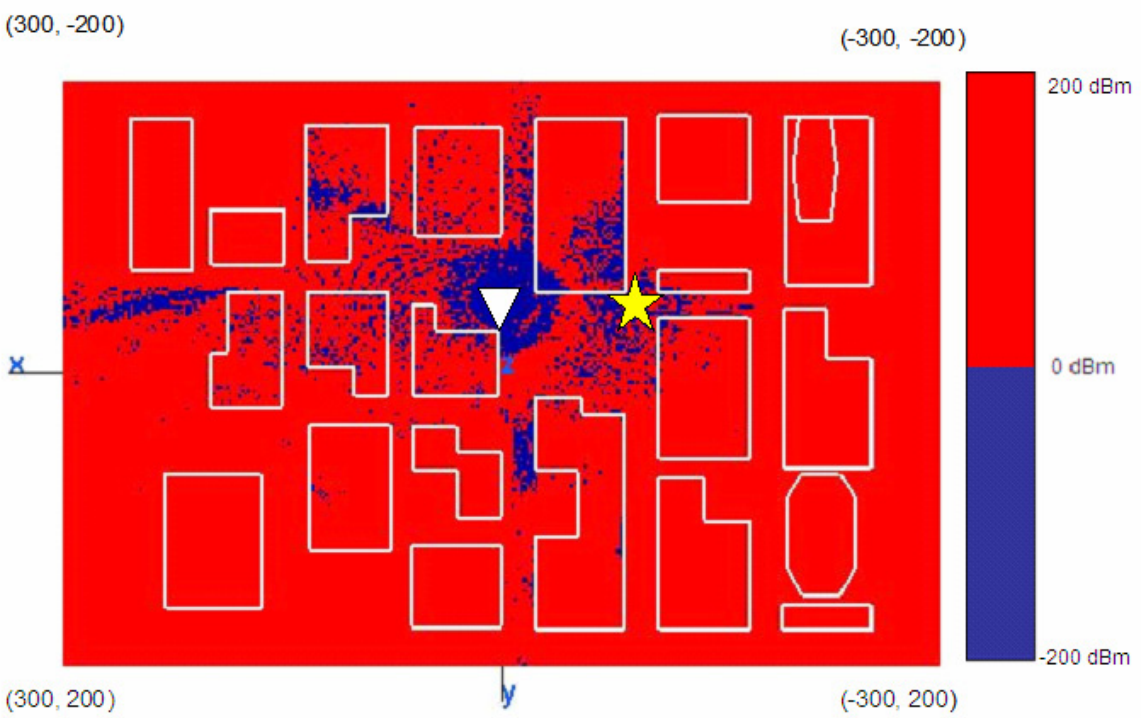

Figure 43. Signal-to-Jam Ratio for 1 W Transmitted (Vertical Polarization)

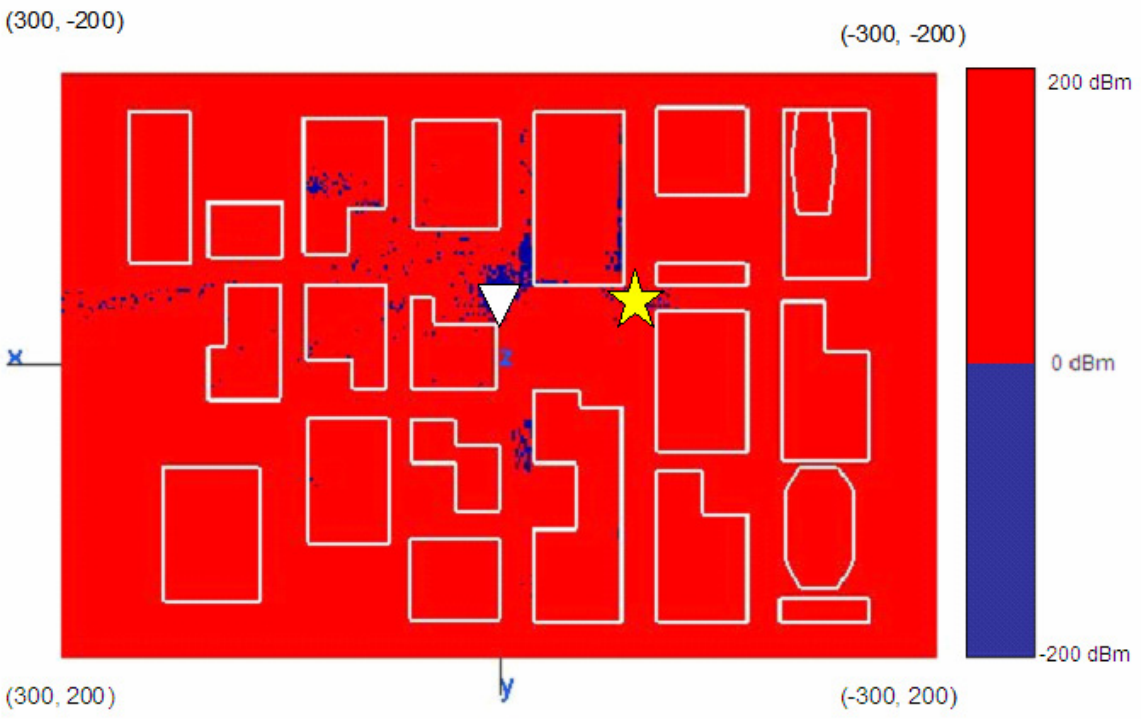

Figure 44. Signal-to-Jam Ratio for 5 W Transmitted (Vertical Polarization)

Figure 45. Signal-to-Jam Ratio for 25 W Transmitted (Vertical Polarization).

The percentages of the links established and jammed are given in Table 16 for better interpretation of the figures.

Power Level	Number of Points			Percentage (%) of Links Established	Percentage (%) of Links Jammed
	-100 to 0 dB	0 to 100 dB	100 to 200 dB		
1 W	3794	56673	34	94.0	6.0
5 W	692	59774	35	98.9	1.1
10 W	295	60171	35	99.5	0.5
15 W	186	60279	36	99.6	0.4
25 W	100	60362	39	99.8	0.2

Table 16. Percentages of Links Established and Jammed at Different Transmitter Power Levels.

As expected, increasing the transmitter power has a positive effect on dealing with the jammer. The percentage of links that can be established increases from 94% at 1 W to 99.8% at 25 W. Data links can be established over a wider area. However, the UAV becomes more susceptible to detection since it radiates more power. Furthermore, it may not be practical to design a vehicle that can carry the large heavy transmitter units necessary for generating the power. It would also drive up the cost of a vehicle that is supposed to be low cost and expendable. Even though it gives better results in simulations, the power level should be as low as possible in real world applications.

The results shown in Figures 42 through 44 above are favorable to the ground troops. The enemy may want to increase power to improve the jamming. Power increase has a dramatic effect on jamming. Table 17 summarizes the effect of jammer power on a 1 W transmitter. The locations are kept the same as for the last series of simulations (UAV at Location 5).

Jammer Power Level	Number of Points			Percentage (%) of Links Established	Percentage (%) of Links Jammed
	-100 to 0 dB	0 to 100 dB	100 to 200 dB		
1 W	3794	56673	34	94.0	6.0
10 W	14280	46187	34	76.4	23.6
50 W	22285	38182	34	63.2	36.8
100 W	25761	34706	34	57.5	42.5

Table 17. Percentages of Links Established and Jammed at Different Jammer Power Levels.

Figures 45 through 48 illustrate the jammer's effectiveness when it increases its power.

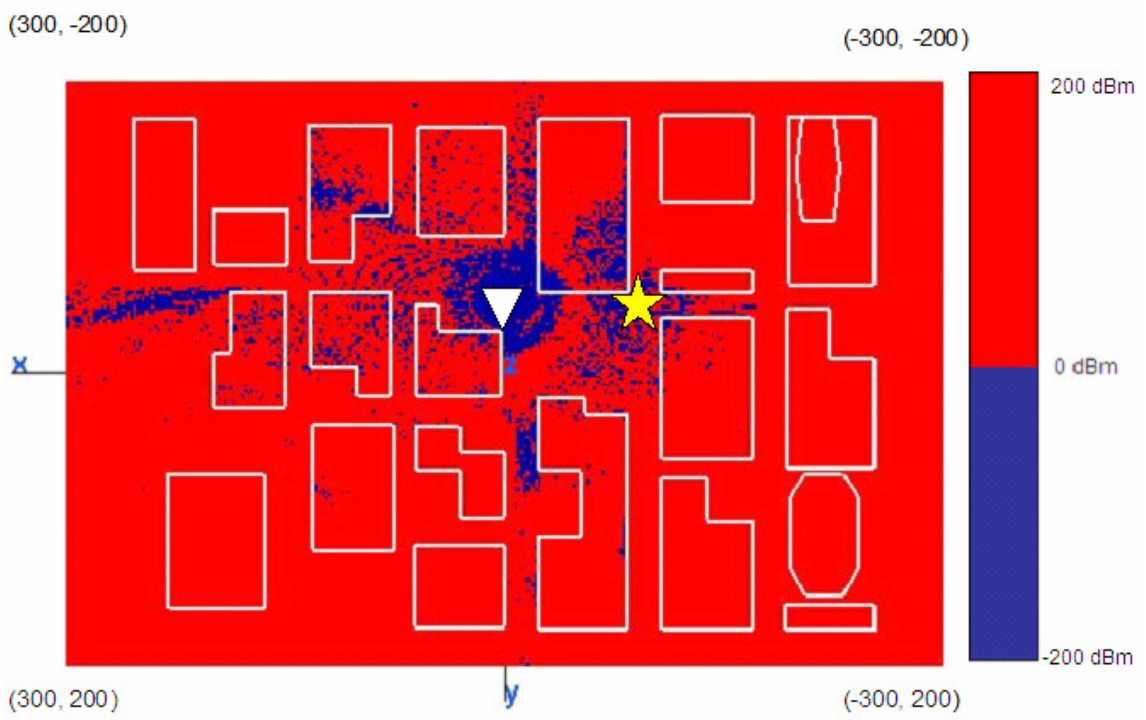

Figure 46. Signal-to-Jam Ratio for 1 W Jammer (Vertical Polarization).
Figure 47.

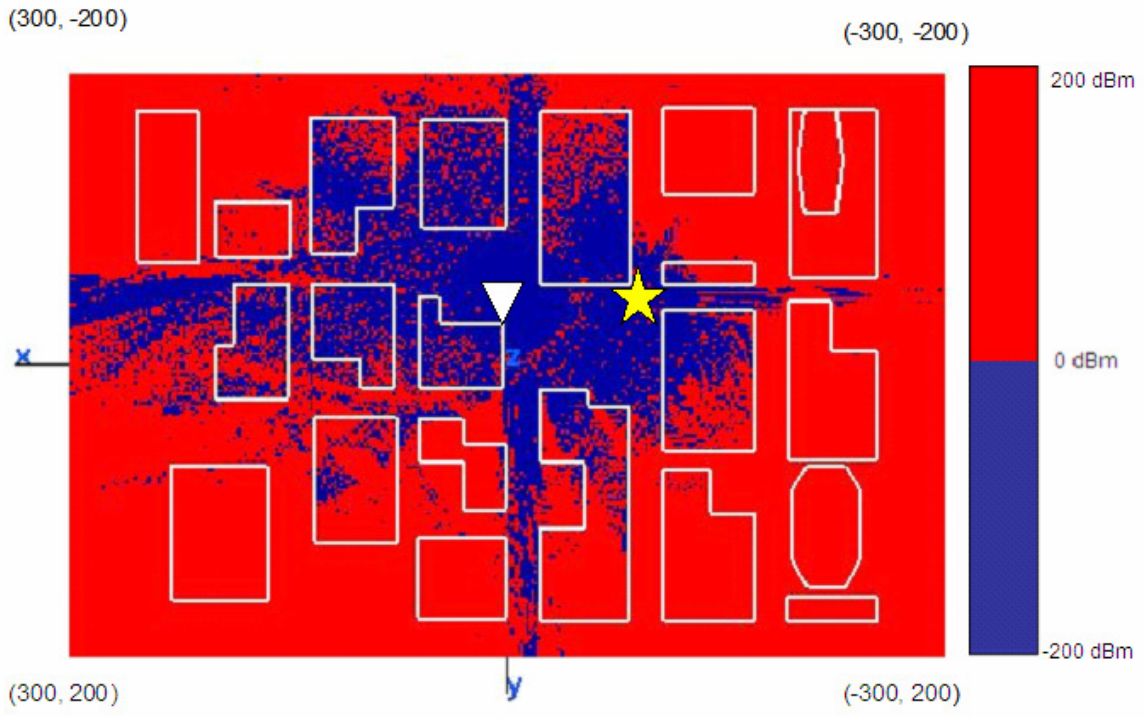

Figure 48. Signal-to-Jam Ratio for 10 W Jammer (Vertical Polarization).
Figure 49.

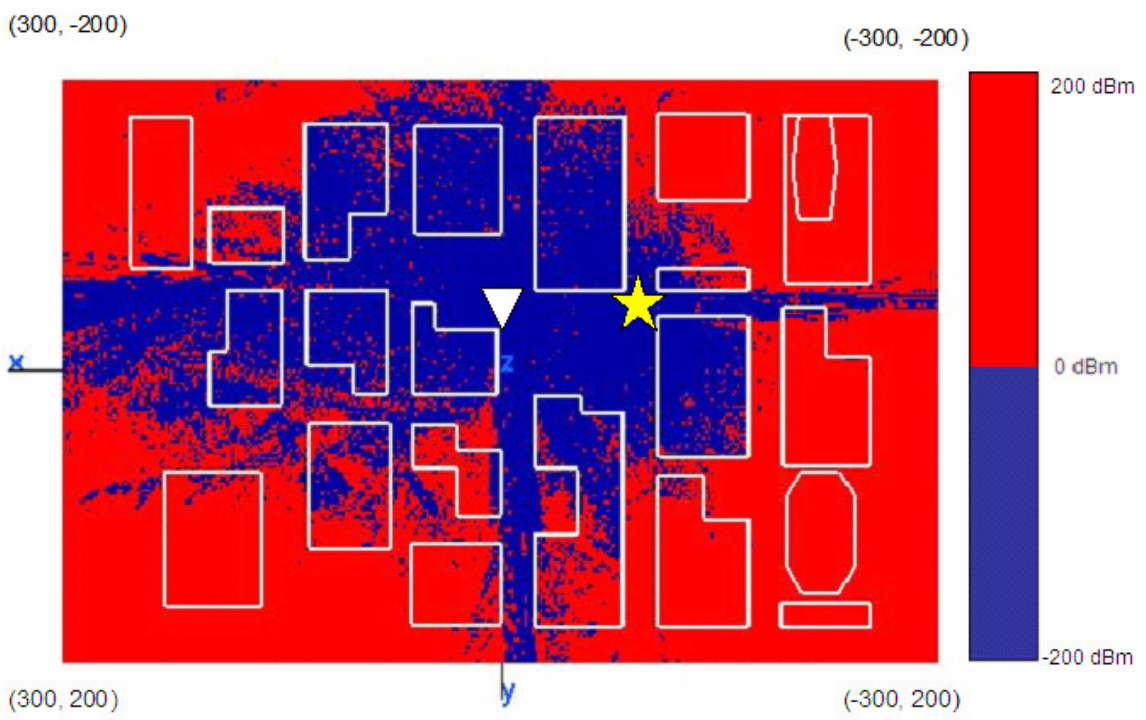

Figure 50. Signal-to-Jam Ratio for 50 W Jammer (Vertical Polarization).
Figure 51.

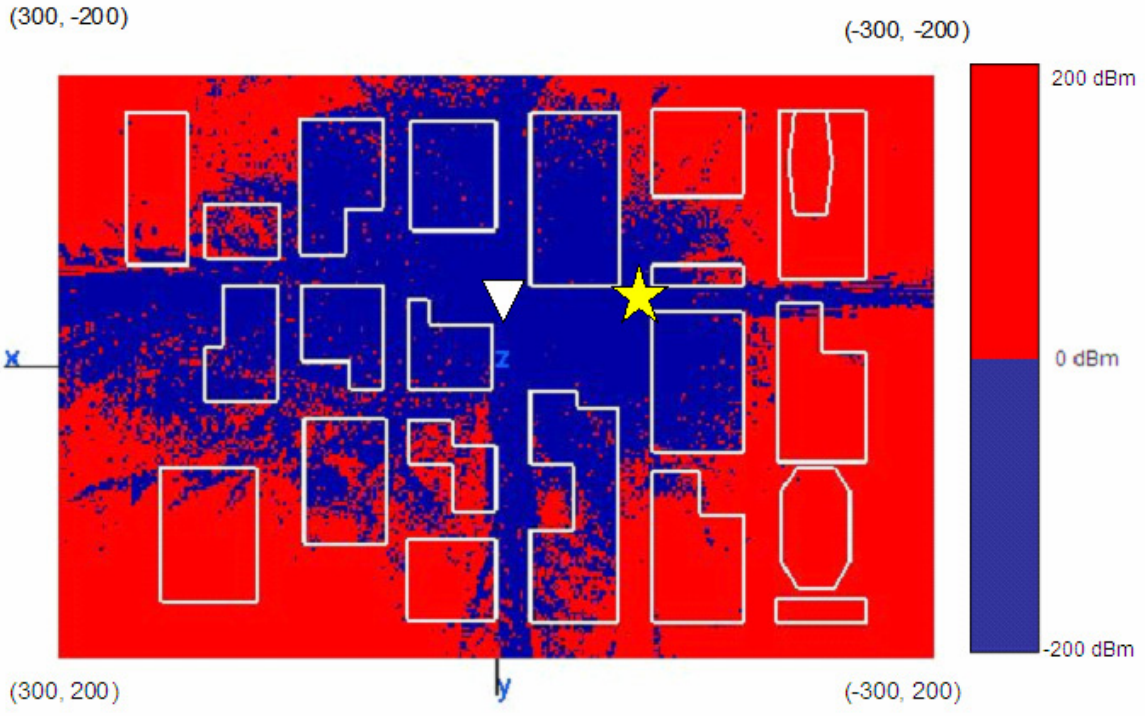

Figure 52. Signal-to-Jam Ratio for 100 W Jammer (Vertical Polarization).
Figure 53.

D. SUMMARY

In this Chapter, the characteristics of urban radio wave propagation and the effectiveness of diversity techniques on the link performance against jamming were simulated and examined. Polarization diversity, frequency diversity and different transmitter power levels were examined. A vertically polarized transmitter had higher percentages of links that could be established for every location taken on the flight path. The highest percentage that could be obtained was 94%. Lower frequencies had better performance compared to higher frequencies. High frequencies were more attenuated in lossy materials like concrete, which was used for the buildings in this study. Last, increasing the transmitter power had a positive effect on dealing with the jammer. The percentage of links that could be established increased from 94% at 1 W transmitted to 99.8% at 25 W transmitted.

V. CONCLUSIONS AND FUTURE WORK

A. CONCLUSIONS

Communications have always been a serious issue in MOUT. Besides the power constraints associated with man-portable radios, fading, path loss and Non-Line of Sight situations, there are additional issues presented by the enemy. Jamming of radio links is one of them. Since the UAVs are often used as communication relays these days, the links between UAVs and the ground units fighting in the city have become a prime target for jamming. Different diversity techniques can be used in overcoming the jamming effects.

In this thesis, mainly two diversity techniques were studied. They were polarization diversity and frequency diversity. Additionally, different transmitter and jammer power levels were examined to see the effects on the communication link. In the scenario, it was assumed that the friendly forces fighting in the city owned the UAV relay and the enemy defended the city and used the jammer to jam the ground receiver. *Urbana* was used to model the scenario and to calculate the link efficiency (availability) in each case. The results can be summarized in the following paragraphs.

Even though there was no dramatic difference between the two polarization types, a vertically polarized transmitter had higher percentages of links that could be established for every location taken on the flight path. The highest percentage that could be obtained was 94% for vertical polarization and 93.1% for horizontal polarization. However, there may be some real life scenarios where varying antenna polarization can provide more reliable links.

Lower frequencies had better performance compared to higher frequencies. High frequencies were more attenuated in lossy materials like concrete, which was used for the buildings in this study. Furthermore, the path loss $\left(\lambda/4\pi R\right)^2$ increases with frequency. This decreases the received power because the antenna gains are assumed constant (i.e., half-wave dipoles). The percentage of good links was at the highest level of 93.7% for the center frequency of 0.9 GHz. It was reduced to 91.6% at 2.4 GHz, and it reached a low of 89.7% at the center frequency of 5 GHz. However, higher frequencies may be

preferred since they have an advantage of higher data rates compared to lower frequency bands. There is a tradeoff in this regard.

As to transmit power issue, increasing the transmitter power had a positive effect on dealing with the jammer. The percentage of links that could be established increased from 94% at 1 W to 99.8% at 25 W. But the UAV became more susceptible to detection since it radiated more power. Furthermore, it may not be practical to design a vehicle that could carry the large heavy transmitter units necessary for generating the power. It would also drive up the cost of a vehicle that is intended to be low cost and expendable.

A final point to note is that even though the ground jammer is not all that effective, it could concentrate its energy on the UAV receiver and probably be more disruptive. Although two-way links would be interrupted the downlink portion will still function. The UAV transmitter could still send information and commands one way to ground troops without interruption.

B. FUTURE WORK

Future work would be valuable in the following areas:

- Effectiveness of space diversity and angle diversity against a jammer could be examined.
- A more sophisticated jammer may be modeled, such as different antenna types (a directional antenna).
- A specific city could be studied. It may be one that has a potential for conflict in the future (they may be the cities in Iraq and Afghanistan).
- Model a jammer directed at the UAV receiver.

APPENDIX A. URBANA INPUT SCRIPT FILE

The following is the sample *Urbana* input file used for simulations.

```
--- input Urbana v 2.5
#
# ********************************
# A---scatterer file,length & freq
# ********************************
#--- name of scatterer file in ACAD format (e.g. wall.facet)
filename.facet
#--- length unit:1=inch, 2=cm, 3=meter, 4=mm, 5=mil
3
#--- uniform freq (GHz): start freq, end , nstep
# (nstep=0 means: just do first freq. CAUTION: antenna patterns are
# assumed to be indep. of freq and is calculated at end freq)
0.875 0.875 0
#
# **********************************
# B--- Antenna Description and List
# **********************************
#
#---Enter method of describing antennas.
# (1 = here, 2 = file):
2
#---If described in file, enter file name:
filename.antenna
#---If described here, fill in sections B1, B2, B3.
# If described in file, use dummy data in sections B1, B2, B3
# (specify one dummy antenna type, dummy antenna origin,
# and one dummy item in antenna list).
#
# ************************
# B1: Define Antenna Types
# ************************
#
# Two lines for each type.
# Line1: type ID, ant code
# Line2: parameters
#
# Type ID must start from 1 and increment by 1 thereafter
#
# Ant Code meaning parameters
# -------- ---------------- ----------------------------
# 1 pattern file filename(ascii)
```

```
106
# 2 dipole length(real)
#
# Antenna Types list:
#
# Enter number of antenna types:
1
# Type #1
1 2
0.1714
#
# ************************************************
# B2: Enter origin of antenna coord in main coord
# ************************************************
#
0. 0. 0.
#
# ************************
# B3: Create Antenna List
# ************************
#
# Three lines for each antenna.
# Line1: Type ID, location (x,y,z), power (watts), phase(deg)
# Line2: Local x-axis in main coord.
# Line3: Local z-axis in main coord.
#
# Enter number of antennas:
1
#
# Antenna #1
1 -10 -55 150 1. 0.
1. 0. 0.
0. 0. 1.
#
# ***********************
# C---Observation points
# ***********************
#--- Observation points defined with respect to main coord. system 7.
# Enter method of specifying list of points.
# (1 = here, 2 = file):
2
#--- If points are listed here, enter number of points (kobtot):
1
#--- If listed here (1 above), List xyz of points in main coord 7
# (one point at a line). If 2 above, include one dummy line.
1. 2. -11.00
```

```
#--- If points listed in file (2 above), enter name of file.
107
observationplane.list
#--- Include direct Tx to observer contribution.
# If you turn on the direct contribution from the transmitter to the
# observation point, computed result will be the total field, which is
# the incident + scattered field. For propagation analysis, this is
# the preferred setting. Otherwise, the result only includes the
# scattered field.
#
# Include direct contribution from transmitter to observation point (rx)
# (1 = yes, 0,2 = no):
1
#--- Compute received power into Rx antenna.
# Urbana always computes field levels at the observation point.
# If you specify an Rx antenna, Urbana will also compute the received
# power and record the results in the (runname).couple file.
# This causes a moderate but slow-down when using the SBR method (below).
#
# Include Rx antenna (1 = yes, 0,2 = no):
0
#--- Rx antenna specification
# Remaining entries in Section C can be ignored if not including
# an Rx antenna.
# Enter antenna type (1 = pattern file, 2 = dipole):
1
# Each antenna type requires additional parameters.
# List of expected parameters follows. Choose one.
#
# Type Description Expected Parameter(s)
# 1 Pattern File File Name (e.g., beam.antpat)
# 2 Dipole Length (in prevailing unit)
#
# Enter parameter(s) on next line:
dummy.antpat
#--- Rx antenna orientation
# Enter local x-axis of Rx in global coordinates
1. 0. 0.
# Enter local z-axis of Rx in global coordinates
0. 0. 1.
#
# ****************************
# D---Theoretical consideration
# ****************************
#--- Choose method of computation
# 0 = compute fields in the ABSENCE of the scatterer
```

```
# 1 = compute fields by SBR
# 2 = compute fields by GO
108
2
#--- If SBR, select a PO integration scheme at bounce points
# 1 = do integration at first & last bounce points only
# 2 = do so at all bounce points (GTD formulation)
1
#--- Edge diffraction
# SBR can be enhanced with PTD edge diffraction.
# GO can be enhanced with GTD edge diffraction.
# Add edge diffraction (0,2=no, 1=ILDC (SBR or GO), 3=UTD (GO only)
3
#--- If edge diffraction switched on, enter name of edge file
# (e.g., wall.edge or dummy if edge not included).
filename.edge
#--- Choose method of ray launch
# 1 = by (baby) facet, achieving a uniform first bounce surface density
# 2 = uniform angular distribution (burst launch)
# (If computation by GO, must select 2 = burst launch)
2
#--- If ray launch by (baby) facet (1 above), enter ray density:
# # rays/wavelength (normally 5-10)
5.
#--- If burst ray launch (2 above), enter angular interval (deg).
# (Typically 0.25 - 2.0 deg)
2.
#--- max permissible ray bounces (normally 5-10)
7
#--- max-voxdepth = max depth of BSP tree (normally 20)
# max-voxl = max facets in each voxel(normally 10)
# (Larger voxdepth & smaller voxl lead to faster ray tracing
# but more computer memory)
20,10
#--- ICOAT for absorbing facets
888
#--- IQMATRIX for divergence factor
# 1 = calculated by Q-matrix
# 2 = ignored except for the spherical wave spread
2
#--- IF using Q-matrix, name target curvature file(e.g. wall.curv)
dummy.curv
#--- IPEC=1 if all pec, =2 if coating present
2
#--- For PEC scatterer, give the magnitude of reflection coeff
# (use 1.0 for ideal PEC, use less for rough PEC--fudging)
```

```
1.0
#--- IF PEC, the rest coating info is dummmy
#--- material reflection is done through a look-up table
109
# specify the freq interval in GHz for the table e.g. 0.25
# (dummy if input freq less than 51)
0.2
********************
E---coating material
********************
---- number of materials
(NOT including pec, which is identified by ICOAT=0)
(NOT including absorbing facets: ICOAT=28 or 888)
(If 3 material, urbana reads only ICOAT=1-3)
3 <----NCOTOT
--- for each material, identify its boundary type:
iboundary = 1 if impedance boundary
2 if layered slabs with PEC backing
3 if penetrable layered slabs with air backing
4 if penetrable FSS Tx/Refl table supplied by user
5 if same as 2 except using freq-dep ramlib.d
6 if antenna refl table supplied by user
7 if layers over semi-infinite ground
for each material, given info by following the templates
^^^ ICOAT=1 ^^^^^^^^^^^^^^^^^^^^^^^^^^^^^^^^^^^^^^^^^^^^^^^^^^^^^^^
--- iboundary
3
--- number of layers over air backing
(1st layer is farthst fr incid field and innermost)
1
--- thick,epsilon(c),mu(c),resistivity(ohm)
0.30000 (10.1,0.5) (1.0,0.0) 1.e+30
^^^ ICOAT=2 ^^^^^^^^^^^^^^^^^^^^^^^^^^^^^^^^^^^^^^^^^^^^^^^^^^^^^^^
--- iboundary
2
--- number of layers over PEC backing
(1st layer is farthst fr incid field and innermost)
2
--- thick,epsilon(c),mu(c),resistivity(ohm)
0.0300 (2.5,-0.000) (1.6,-0.000) 1.e+30
0.0500 (3.0,-0.000) (1.0,-0.000) 1.e+30
^^^ ICOAT=3 ^^^^^^^^^^^^^^^^^^^^^^^^^^^^^^^^^^^^^^^^^^^^^^^^^^^^^^
--- iboundary
7
--- number of layers over half-space (semi-infinite ground)
(1st layer is farthst fr incid field and innermost)
```

```
1
--- thick,epsilon(c),mu(c),resistivity(ohm)
0.1000 (3.000,-0.0) (1.0,-0.0) 1.e+30
--- epsilon(c),mu(c) of semi-infinite ground
110
(3.00,-0.00) (1.0,-0.00)
(End of regular input file. Leave a few blank lines)
-----------------------------------------------------------------
'OPTIONAL ADVANCE FEATURES' (Do not change letters in quotations)
# The line above must be placed at the end of the regular urbana
# input. Advance features are designed for special applications or
# for testing codes. They are not needed by general usages.
# ------------------------------------
# ADVANCE1: ADD GTD-TYPE BLOCKAGE CHECK
# ------------------------------------
# In regular urbana computation, blockage check is mostly done by
# PTD principle. For interior scattering in a confined region, use of
# GTD principle may be more appropriate.
# Option to use GTD principle: 1=yes, 2=no (regular case)
2
# ---------------------------------------
# ADVANCE2: SIMPLE TERRAIN BLOCKAGE MODEL
# ---------------------------------------
# For GO method, terrain generates 100% blockage, and blocked rays leave
# no energy behind a hill. With this feature, LOS rays and UTD edge
# diffraction rays can pass through terrain, with some attenuation.
# Attenuation is measured in dB per hill. Each hill is identified
# by two passages through two terrain facets.
# Can only be used with GO method (and UTD edge option).
# Use simple terrain model: 1 = yes, 2 = no (regular case)
2
# Enter coating code range of terrain facets (e.g., 1, 2):
1 1
# Enter amount of attenuation per hill (dB, > 0):
5.
# -----------------------------------------------
# ADVANCE3: APPROXIMATE DOUBLE DIFFRACTION MODEL
# -----------------------------------------------
# For GO + UTD method, only single diffraction is considered.
# With this feature, double diffraction is approximated by identifying
# surfaces which block the single diffraction, such as building walls.
# If one or two facets block the path from the single diffraction point
# to the transmitter, the diffraction is still included, but with attenuation.
# Works best if "diffracting facets", marked by their coating code, are
# always associated with enclosed structures with well defined edges.
# Use double diffraction model: 1 = yes, 2 = no (regular case)
```

```
2
# Encounter coating code range of diffracting facets (e.g., 5, 10):
2 2
111
# Enter amount of attenuation for second diffraction (dB, > 0);
10.
# ----------------------
# ADVANCE4: ACCELERATION
# ----------------------
# For large scenes, run time grows both with the number of field
# observation points and the number of edges. Normally, all combinations
# of lit edges and observation points are considered. This feature
# accelerates the processing by limiting the scope of considered edge
# interactions to region around the LOS path from the transmitter
# to the observation point. For example, to run a 5 km by 5 km scene,
# one may choose a 250 m interaction radius. For each observation
# point, edges are ignored that lie outside an ellipse whose foci are the
# Tx and the observation point and whose major axis is the LOS distance
# plus 500 m (radius x 2).
# This feature can also be used to automatically filter edge files
# whose domain far exceeds the domain of ovservation points.
# Only use this feature for terrestrial simulations where the scene
# is nominally parallel to the x-y plane.
#
# Use large scene acceleration: 1 = yes, 2 = no (regular case)
2
# Enter radius of interaction
250.
# --------------------------
# ADVANCE5: MULTI-DIFFRACTION
# --------------------------
# Subsitute for Adv. #3. Uses ray rubber-banding algorithm to find
# path from transmitter to receiver.
# Can only be used with GO. Cannot be used in conjunction with Adv. #3.
# If UTD switched on above, will take measures not to double count
# single diffraction mechanims.
# Use multi-diffraction model: 1 = yes, 0,2 = no
2
# Enter coating code range of diffracting facets (e.g. 5, 10):
2 2
# Enter maximum number of rubber-band points ( also used in Advance6 )
1
# Check multiple crawl planes instead of just vertical one: 1 = yes, 0,2 = no
0
# --------------------------
# ADVANCE6: REFLECTION-DIFFRACTION
```

```
# --------------------------
# If UTD switched on above, will take measures not to double count
# single diffraction mechanims.
# Use reflection-diffraction model: 1 = yes, 0,2 = no
2
# Do more than just single diffractions: 1 = yes, 0,2 = no
# Allow rubber-banding to both transmitter and receiver: 1 = yes, 0,2 = no
1 0
# Choose crawl plane selection mode: 0 = always vertical, 1 = initial edge,
# 2 = adaptive from edge to edge
1
# ----------------------------------
# ADVANCE7: GREEN'S FUNCTION (GF) FILE
# ----------------------------------
# By default, for SBR and no-target methods, a GF file IS NOT produced.
# Also, by default, for GO, a GF file IS produced.
# Use this feature to explicitily activate or de-activate generation
# of the GF file, which is needed by the re-processor for its activities.
# Activate GF file: 0 = no, 1 = yes, 2 = default activation behavior
2
# If yes, enter buffer scale factor. Increasing scale factor reduces
# the number of GF file dumps to disk during a run, but costs memory.
# Recommend 2 - 5 for GO method, 1 for no-target method,
# and 100 - 10000 for SBR method.
2
```

APPENDIX B. MATLAB CODE

The following is the code used for generation of observation plane.

```
% Observation points generation
%-----------------------------------------------------------------------------------------
clc;
i = 1;
z = 4;
for x = -300:2:300;
    for y = -200:2:200;
        M(i, : ) = [x, y, z];
        i = i + 1;
    end
end
save obvpoint M – ASCII;
%-----------------------------------------------------------------------------------------
```

THIS PAGE INTENTIONALLY LEFT BLANK

LIST OF REFERENCES

[1] *Tactical Battlefield Communications*, Defense Science Board Task Force, Office of the Under Secretary of Defense for Acquisition, Technology, and Logistics, February 2000.

[2] *The Army Digitization Report 2000*, Report on the Plan for Fielding the First Digitized Division and the First Digitized Corps, Presented to the committee on Armed Services, U.S. Senate, Second Session, 106th Congress, April 2000.

[3] Edwards, S. J. A., *Freeing Mercury's Wings, Improving Tactical Communications in Cities*, RAND, Santa Monica, CA, 2001.

[4] Bone, E., and Bolkcom, C., *Unmanned Aerial Vehicles: Background and Issues for Congress*, Report for Congress, Congressional Research Service, The Library of Congress, April 25, 2003.

[5] Schleher, D. Curtis, *Introduction to Electronic Warfare*, Artech House Inc., Norwood, MA, 1986.

[6] Richardson, Doug, *An Illustrated Guide to the Techniques and Equipment of Electronic Warfare*, Arco Publishing, Inc., New York, 1985.

[7] Schleher, D. Curtis, *Electronic Warfare in the Information Age*, Artech House, Inc., Norwood, MA, 1999.

[8] Sen, Cem, *"Digital Communications Jamming,"* Master's Thesis, Naval Postgraduate School, Monterey, September 2000.

[9] Stutzman, Warren L., and Thiele, Gary A., *Antenna Theory and Design*, 2nd Edition, John Wiley & Sons, Inc., 1998.

[10] Jenn, D. C., *Lecture Notes for EC3630, Radio wave Propagation*, available at http://www.nps.navy.mil/Faculty/jenn/EC3630list.html, last accessed on July 2005.

[11] Balanis, Constantine A., *Antenna Theory, Analysis and Design*, John Wiley & Sons, Inc.,1982.

[12] Pala, F., *"Frequency and Polarization Diversity Simulations for Urban UAV Communication and Data Links,"* Master's Thesis, Naval Postgraduate School, Monterey, September 2004.

[13] Siwiak, Kazimierz, *Radiowave Propagation and Antennas for Personal Communications*, 2nd Edition, Artech House, Inc., 1998.

[14] Hata, Masaharu, " *Emprical Formula for Propagation Loss in Land Mobile Radio Services,"* IEEE Transactions on Vehicular Tech., Vol. VT-29, No.3, August 1980.

[15] www.saic.com/products/software/urbana/, last accessed on July 2005.

INITIAL DISTRIBUTION LIST

1. Defense Technical Information Center
   Ft. Belvoir, Virginia

2. Dudley Knox Library
   Naval Postgraduate School
   Monterey, California

3. Chairman
   Information Sciences Department
   Monterey, California

4. Professor David C. Jenn
   Department of Electrical and Computer Engineering
   Monterey, California

5. Professor Daniel C. Schleher
   Information Sciences Department
   Monterey, California

6. 1st Lt. Tuncay Ulama
   Turkish Army
   Ankara, Turkey